

Supplementary Materials and Methods

Recording procedures

The hyperdrive was connected to a multichannel, impedance matching, unity gain headstage. The output of the headstage was conducted via a lightweight multiwire tether cable and through an 82-channel slip-ring commutator to a data acquisition system containing 64 digitally programmable amplifiers (Neuralynx, Bozeman, MT, USA). Unit activity was amplified by a factor of 3000-5000 and bandpass filtered from 600-6000 Hz. Spike waveforms above a threshold set individually for each tetrode by the experimenter (~45-70 μ V) were time-stamped and digitized at 32 kHz. EEG signals, 1 per tetrode, were amplified by a factor of 1000 and recorded continuously between 0 and 475 Hz at a sampling rate of 1893 Hz. The EEG channels were recorded differentially against the reference tetrode in the electrically silent region of the corpus callosum. Light emitting diodes (LEDs) on the headstage were used to track the animal's movements at a sampling rate of 50 Hz.

Spike sorting and cell classification

Spike sorting was performed offline using graphical cluster-cutting software (MClust, A.D. Redish). Clustering was performed manually in two-dimensional projections of the multidimensional parameter space consisting of waveform amplitudes and waveform energies, using autocorrelation and crosscorrelation functions as additional separation tools and separation criteria. All trials on a given day, including resting trials with sleep, were clustered in a single analysis. Putative excitatory cells were distinguished from putative interneurons using differences in spike width, average rate and complex-spike bursting. Interneurons were not included in any of the analyses.

Rate maps for individual units

Position estimates were based on tracking of the LEDs on the head stage connected to the hyperdrive. All data were speed-filtered. Only epochs with instantaneous running speeds of 5 cm/s or more were included in the reference sessions. Tracking artifacts (> 100 cm/s) were excluded. During teleportation trials, the data were excluded if power in the theta band was lower than 500% of the wide-band mean power at any time between 10 s before teleportation and 20 seconds after teleportation. To characterize the spatial distribution of firing for individual cells, the position data were sorted into 30×30 position bins, each of $2\text{ cm} \times 2\text{ cm}$. Firing rate distributions were determined by counting the number of spikes in each bin and dividing by the time spent per bin. Maps for number of spikes and time were smoothed individually using a Gaussian average over the surrounding 2×2 bins. Weights were distributed as follows:

```
box = [0.0025 0.0125 0.0200 0.0125 0.0025;...
       0.0125 0.0625 0.1000 0.0625 0.0125;...
       0.0200 0.1000 0.1600 0.1000 0.0200;...
       0.0125 0.0625 0.1000 0.0625 0.0125;...
       0.0025 0.0125 0.0200 0.0125 0.0025;]
```

Theta rhythmicity

Local EEG traces from unit tetrodes in the CA3 were bandpass-filtered off-line. An acausal (zero phase shift) FFT bandpass filter was applied to the signals. The filter function was constructed using a Hamming window. For the low cut-off frequencies, 5 and 6 Hz were chosen for the stopband and passband, respectively; 10 and 11 Hz were chosen for high passband and stopband cut-off frequencies. The mean power within the theta band was assessed by FFT and compared to the mean power of a wide-band spectrum between 0 and 125 Hz. Trials with epochs in which the

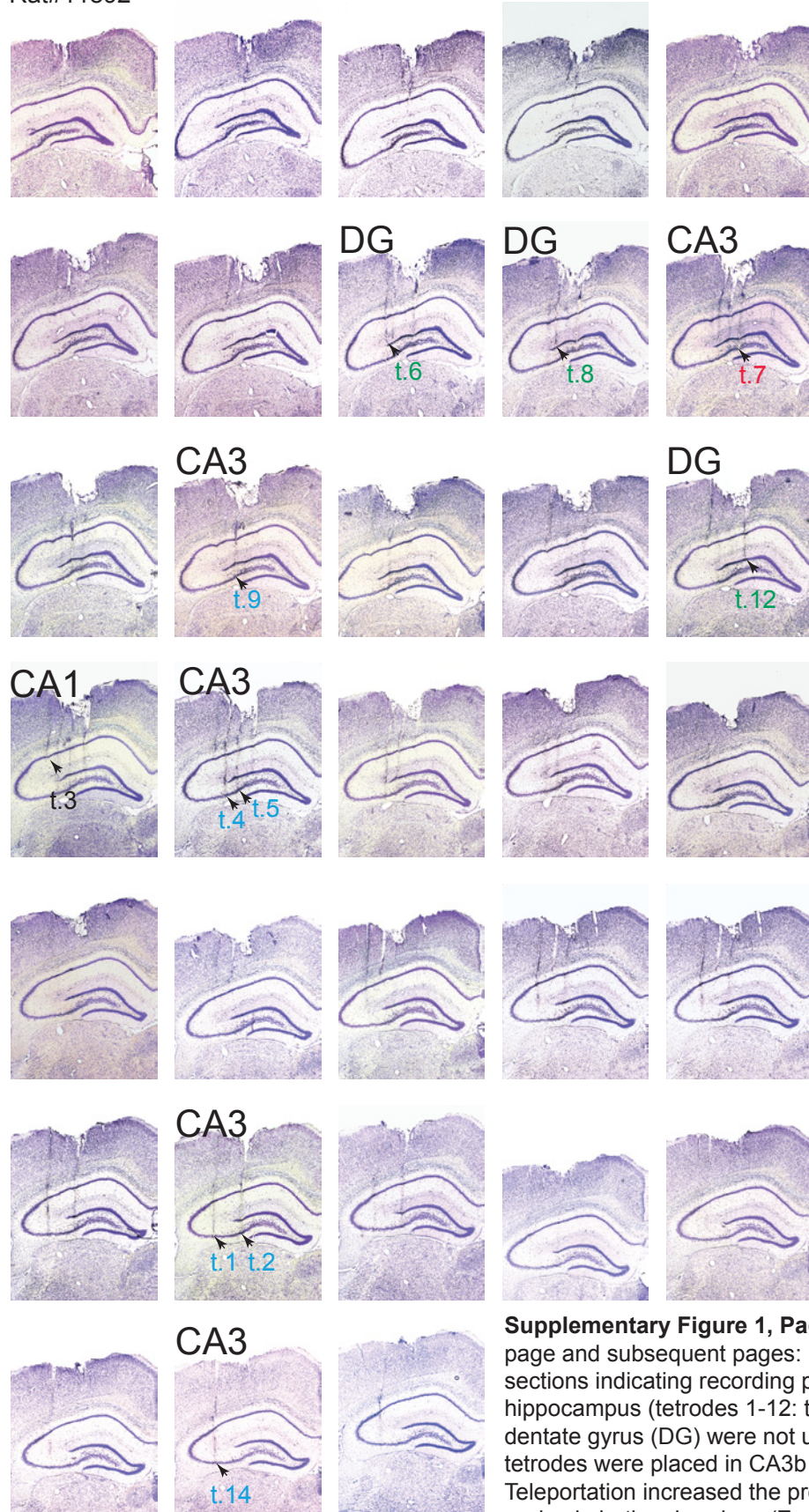
theta band power dropped below 500 % of the wide-band mean power were disregarded in the analysis (20 out of 169 teleportation trials; see main text).

Every recorded spike was assigned a phase relative to the filtered signal, with 0° and 180° referring to the peak and the trough of the signal, respectively. Spike times between peaks and troughs were interpolated linearly between successive peaks and troughs, i.e. the phase assigned to a spike at time t was $180 \times (t - t_0)/(t_1 - t_0)$ where t_0 and t_1 are the times of the preceding and succeeding stationary points (0° and 180° or vice versa) of the filtered EEG signal. Recordings from individual teleportation trials were segmented into successive theta periods, with borders defined by the theta phase with the lowest mean firing rate in the cell sample (Fig. 1bc). Based on this segmentation, a population vector was constructed for each theta cycle from the firing rates of all cells in the trial (Fig. 1c).

Histological procedures and electrode positions

The rats received an overdose of Equithesin or pentobarbital and were perfused intracardially with saline followed by 4 % formaldehyde. The brains were extracted and stored in formaldehyde, and frozen coronal sections (30 μm) were cut and stained with cresyl violet. Each section through the relevant part of the hippocampus was collected for analysis. All tetrodes of the 14-tetrode bundle were identified and the tip of each electrode was found by comparison with adjacent sections. The electrode tip was considered to be located in the section before the tissue damage became negligible. The recordings from a tetrode were included in the data analysis if its deepest position was in the CA3 pyramidal cell layer (or in CA1 in a separate analysis; Supplementary Figure 15). The electrodes had not been moved after the recordings.

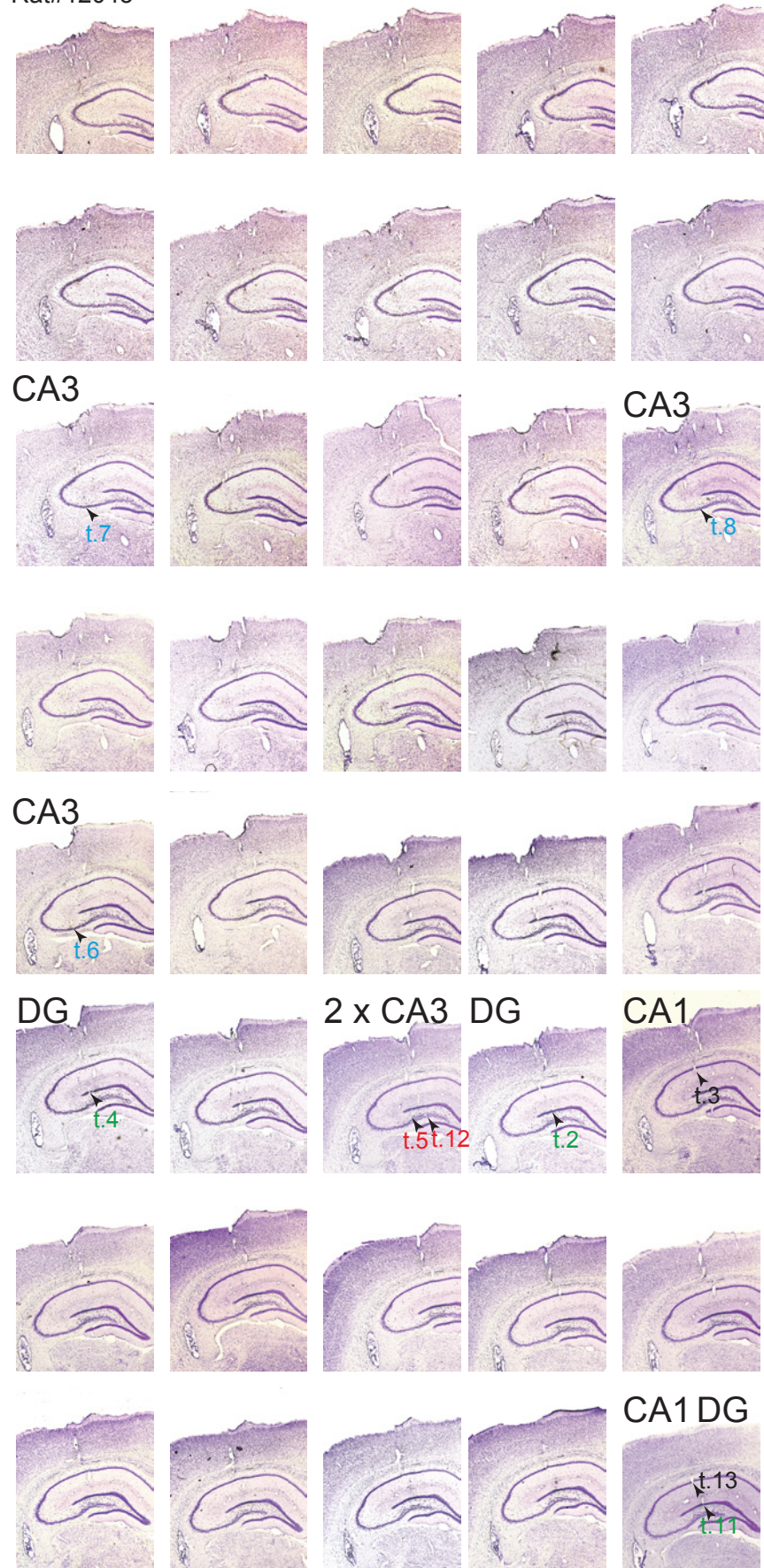
Rat#11892



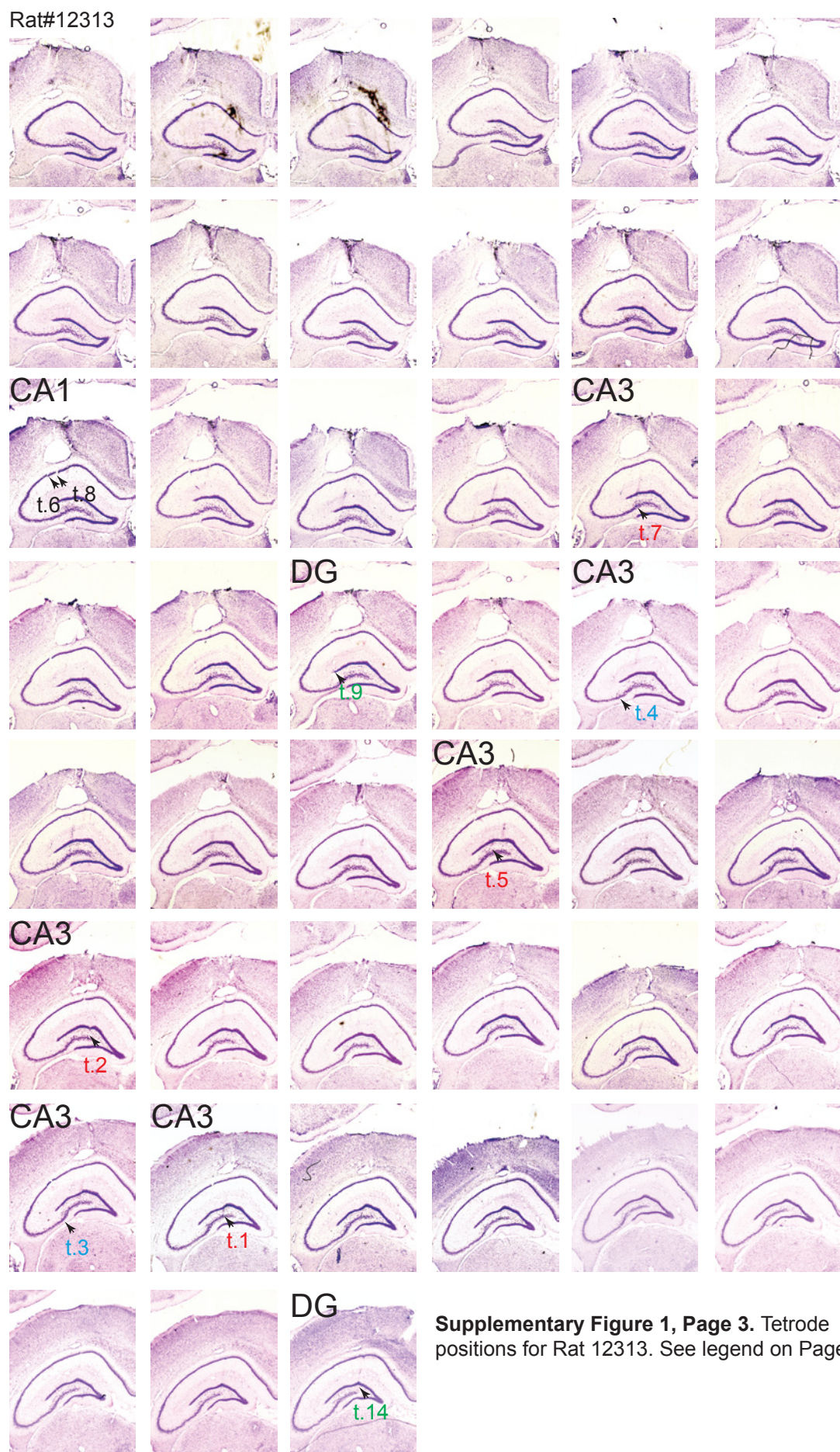
Supplementary Figure 1, Page 1. Tetrode positions. This page and subsequent pages: Nissl-stained coronal brain sections indicating recording positions (arrowheads) in the hippocampus (tetrodes 1-12: t1-t12). Tetrodes in the dentate gyrus (DG) were not used for analysis. CA3 tetrodes were placed in CA3b (blue) or CA3c (red). Teleportation increased the proportion of flicker theta cycles in both subregions ($Z = 12.1$ and $Z = 20.6$, respectively; $P < 0.001$, all trials, all animals, 10 s post-teleportation).

This page shows sections for Rat 11892.

Rat#12045

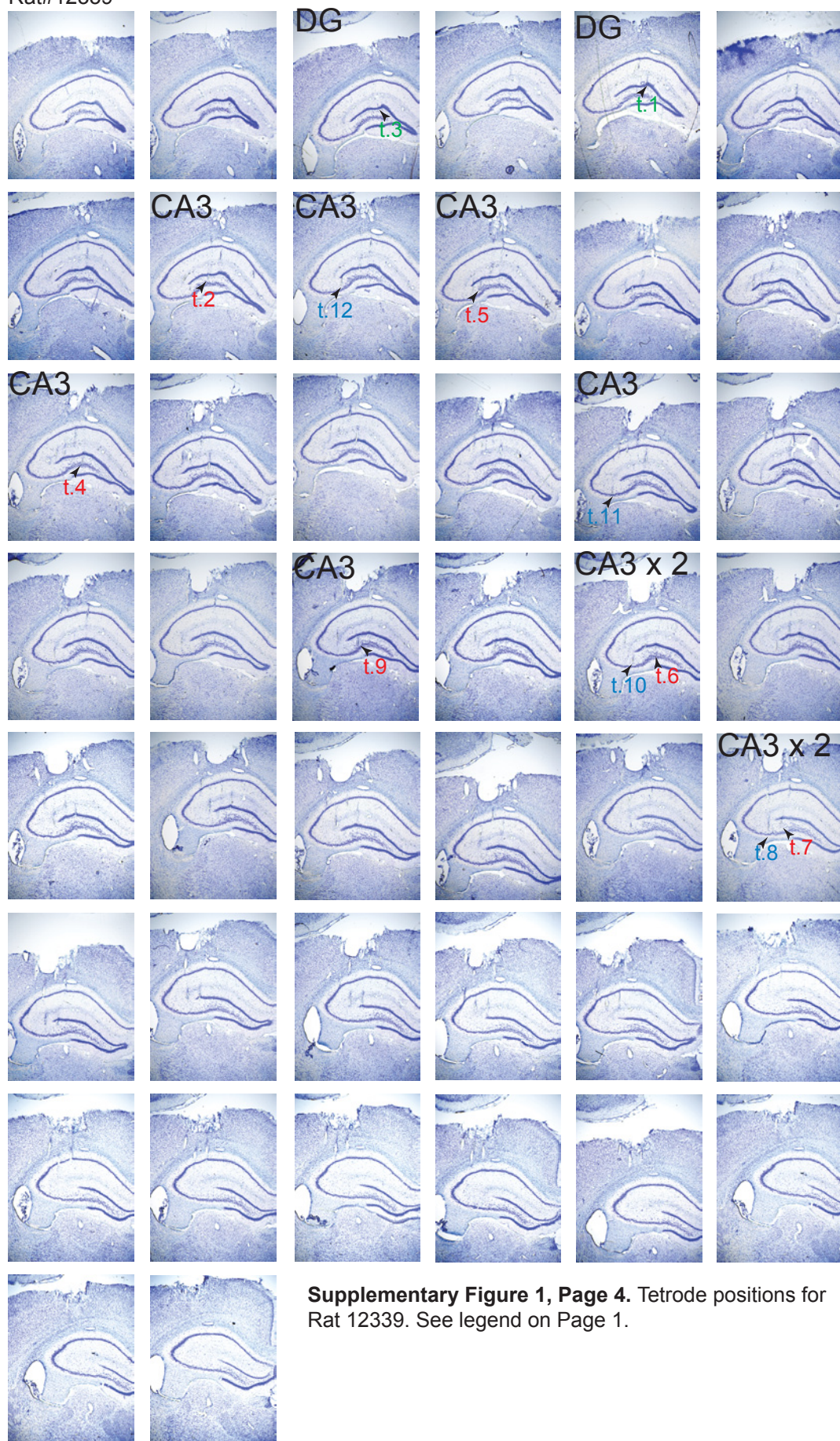


Supplementary Figure 1, Page 2. Tetrode positions for Rat 12045. See legend on Page 1.



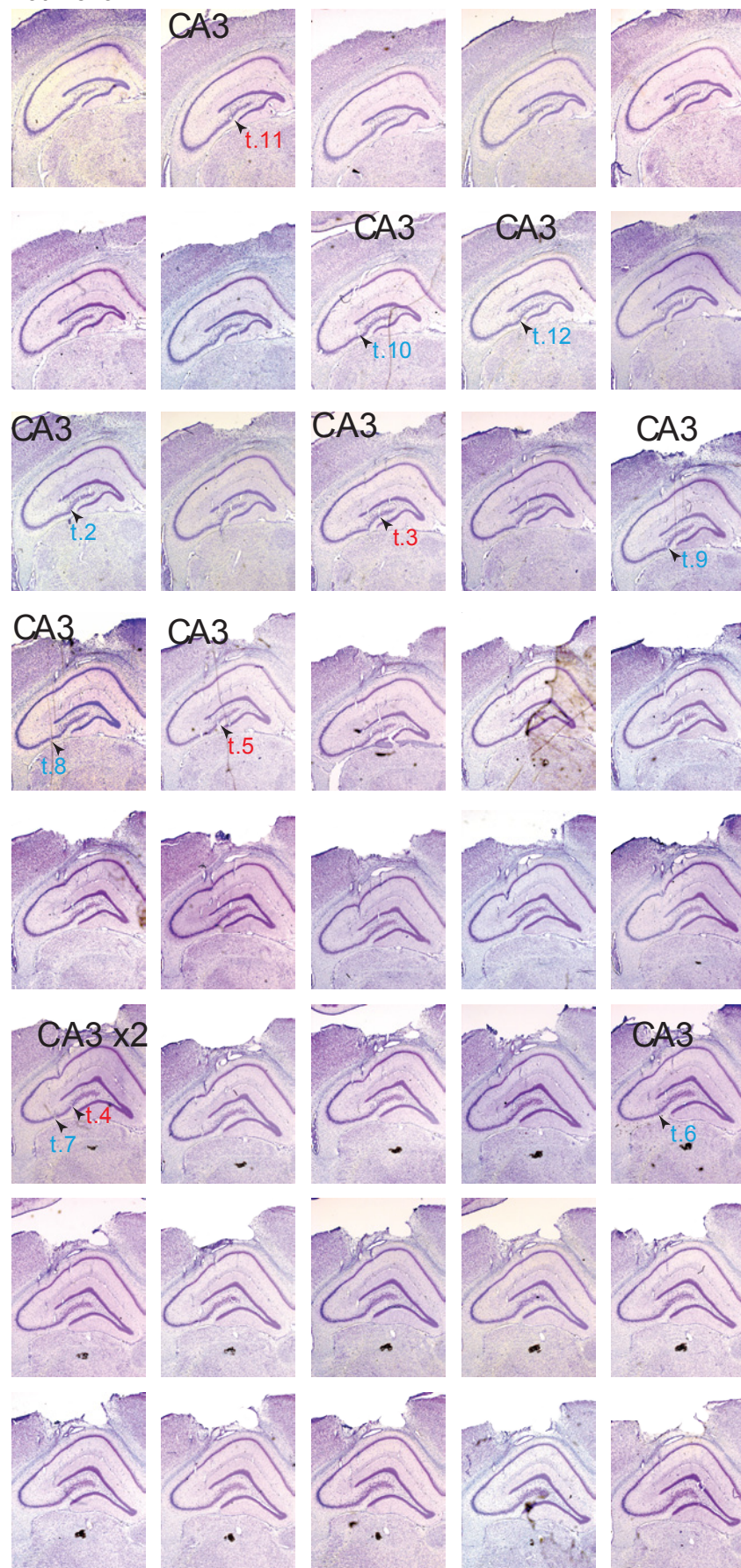
Supplementary Figure 1, Page 3. Tetrode positions for Rat 12313. See legend on Page 1.

Rat#12339



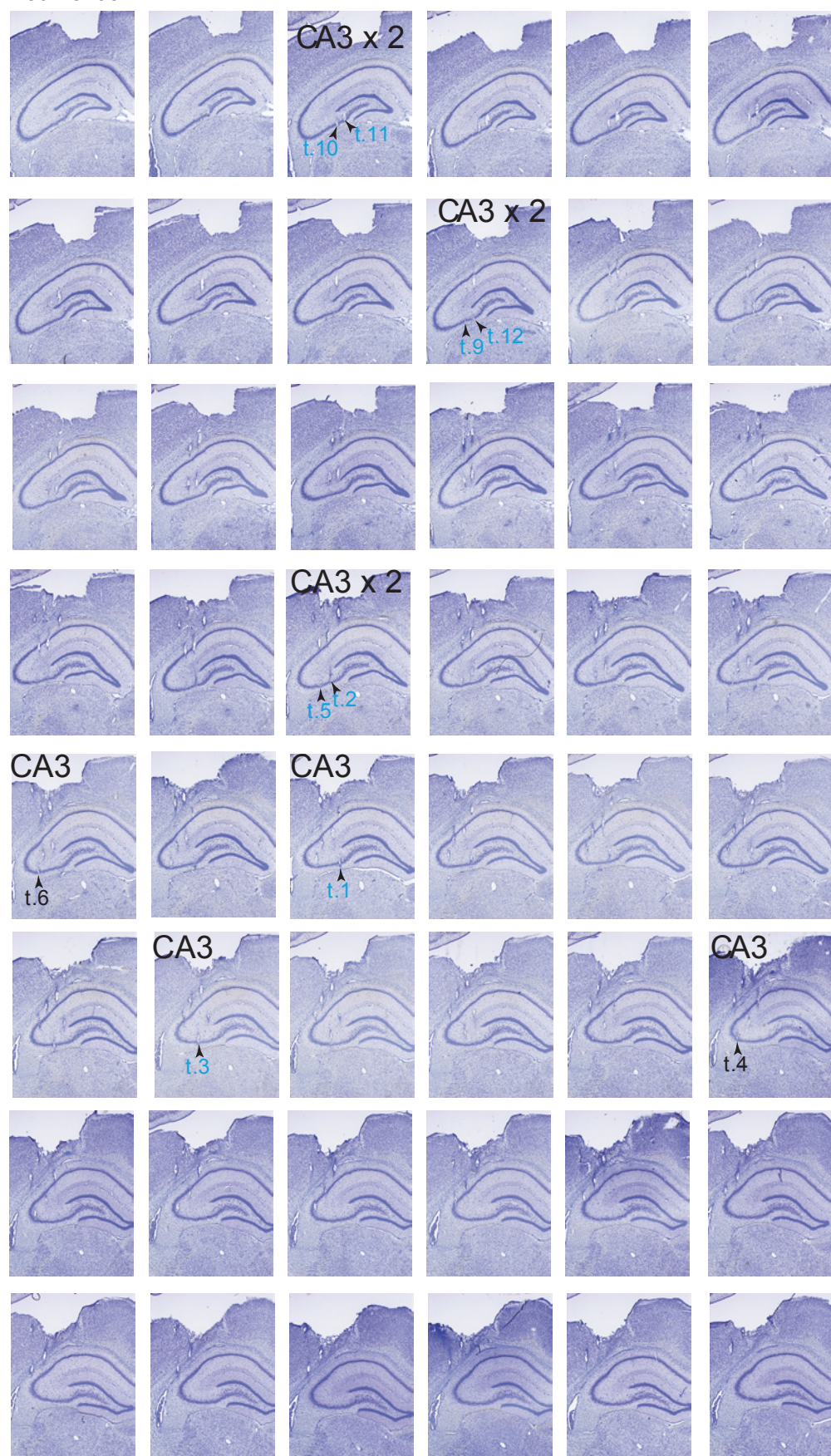
Supplementary Figure 1, Page 4. Tetrode positions for Rat 12339. See legend on Page 1.

Rat#15792

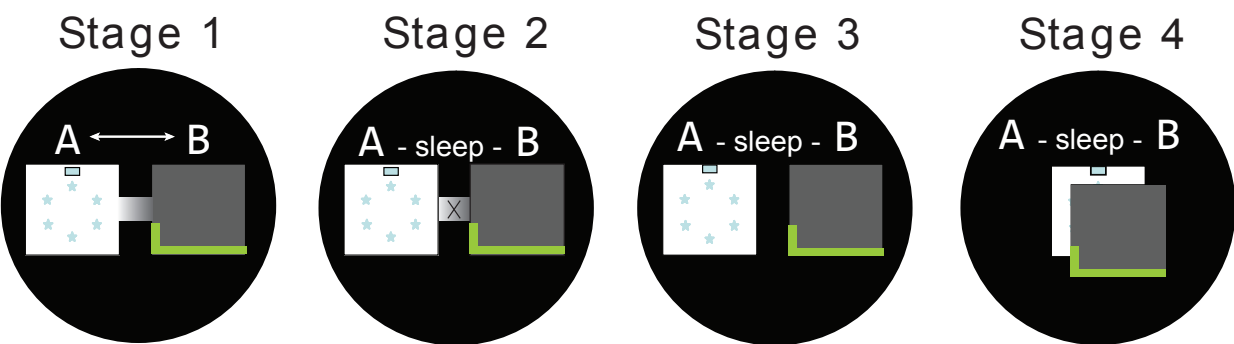
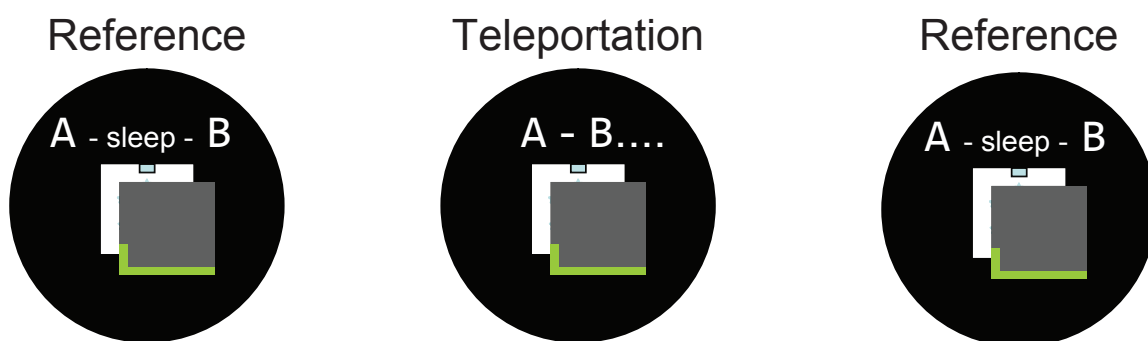


Supplementary Figure 1, Page 5. Tetrode positions for Rat 15792.
See legend on Page 1.

Rat#15793



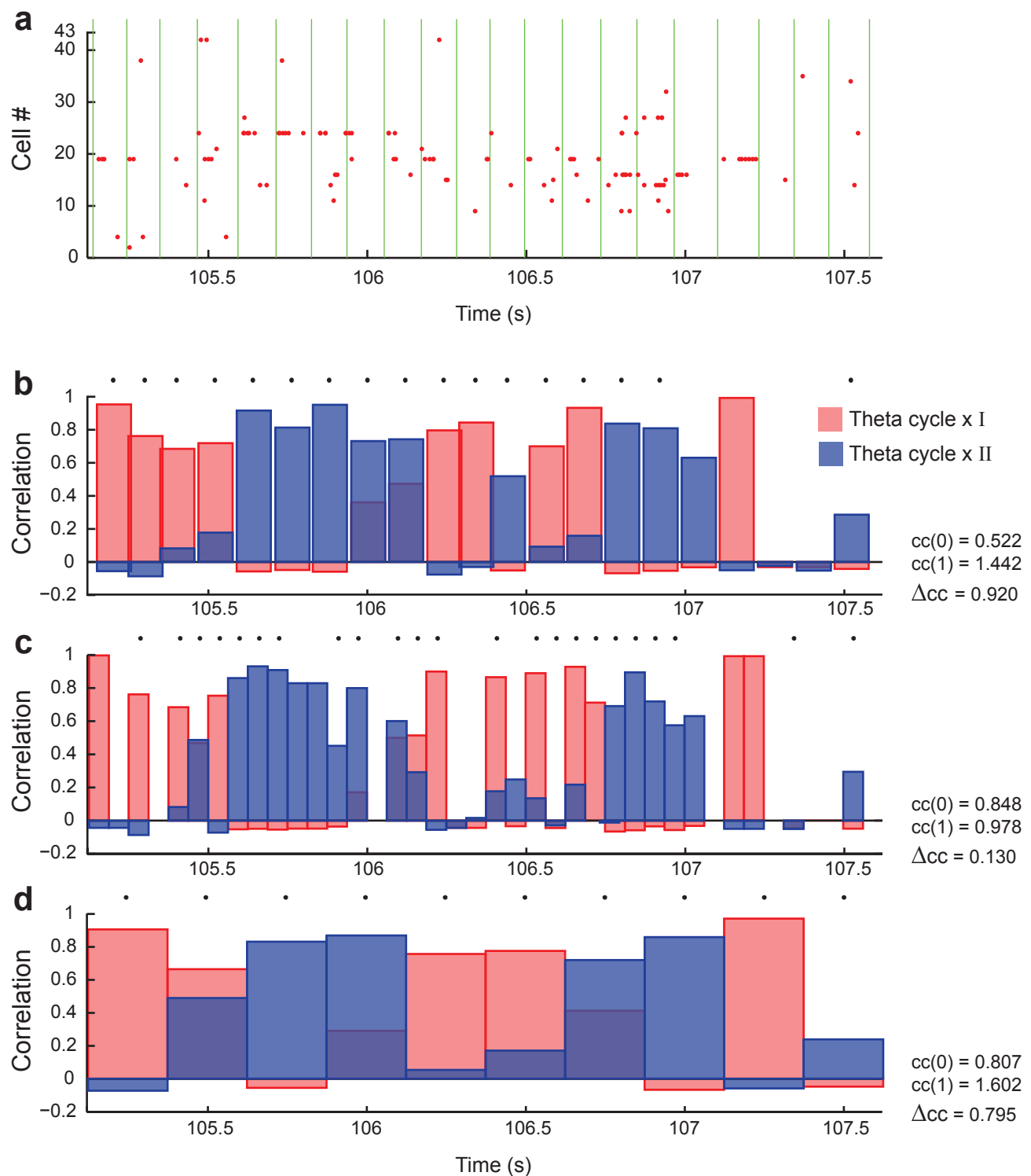
Supplementary Figure 1, Page 6. Tetrode positions for Rat 15793. See legend on Page 1.

TRAINING:**TEST:**

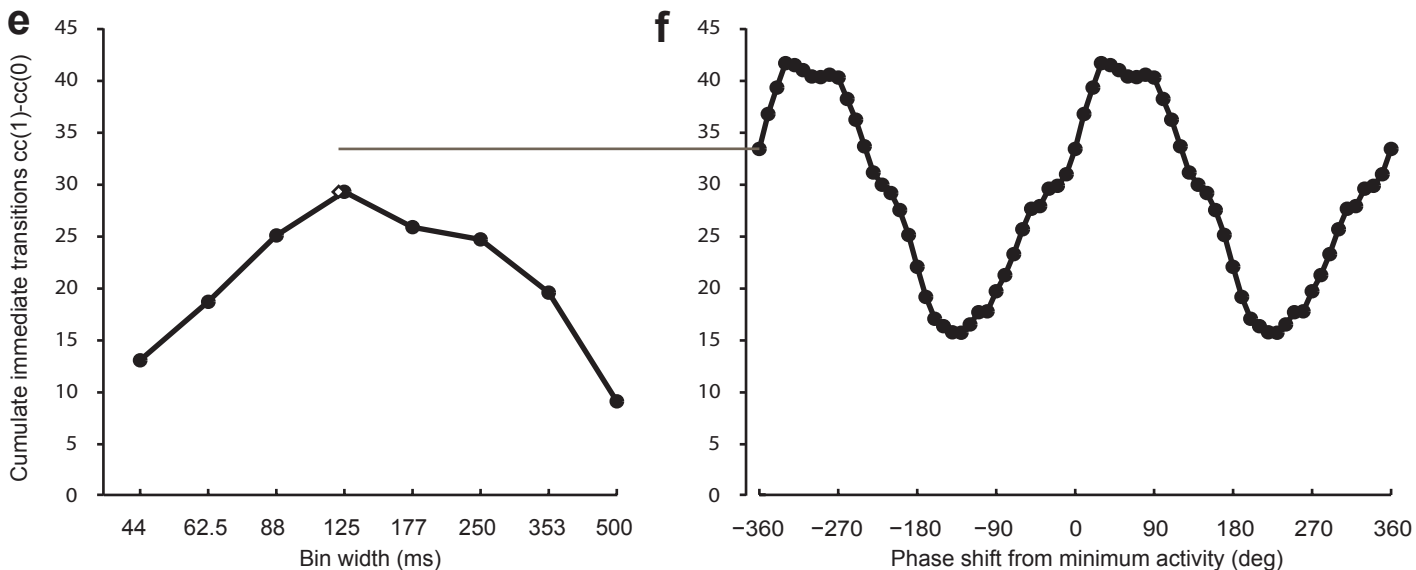
Supplementary Figure 2. *Behavioural training procedure.* Spike-triggered activity and EEG were sampled in either of two distinct 60 cm × 60 cm curtained enclosures with 40-cm walls (Box A and B, respectively). The boxes were identical except for internal lights, which in Box A emerged from dimmed white lamps below the floor (indicated by blue stars), in addition to a polarizing LED at the upper edge of one of the walls, and in Box B came from a series of green LEDs lining the upper edge of two adjacent walls (indicated by a pair of green lines). No other light source was available.

Training occurred in four stages. During Stage 1, the boxes were located next to each other, connected by a passageway that allowed the rat to shuttle between the boxes and associate each box with a different set of path integrator coordinates (ref. 9). The rat was allowed to travel freely between the boxes for 20 min on at least three trials. At Stage 2, the corridor was removed and the animal explored the boxes individually (3 trials in each). At Stage 3, the boxes were replaced by a single box made of the same material and equipped with both sets of lights. The box was placed on alternating trials at one of the two original locations. Finally, at Stage 4, the box was moved to a central location between the two original box locations. The animal received alternating trials with each set of lights. The rat rested in a flower pot outside the enclosures for 20 min between each trial ('sleep' trials). On the teleportation day, the rat was tested first for 10 min in each box configuration (reference trials in A and B, respectively; left). These trials were separated by resting trials in the flower pot ('sleep'). During the third trial (middle), after 40-60 s of recording in one of the box configurations, the lights were switched instantaneously to the alternative configuration. Because no other cues distinguished the environments, the substitution of cues effectively 'teleported' the animal from one box to the other. Additional switches were made every subsequent 40-60 s until 10 min had passed. Finally, the rat was tested again in the reference environments (right).

The training procedure generated discrete place representations in the two environments on the test day. The subset of active CA3 cells on reference trials in the two boxes showed minimal overlap: $61.4 \pm 3.8\%$ of the cells passed a rate threshold of 0.10 Hz in Box A, $62.6 \pm 2.8\%$ in Box B, and only $30.9 \pm 4.1\%$ were active in both environments (means \pm S.E.M.). The mean population vector correlation between the two reference environments, averaged across spatial bins, was 0.013 ± 0.016 , suggesting that the distributions of firing in the two environments were independent.

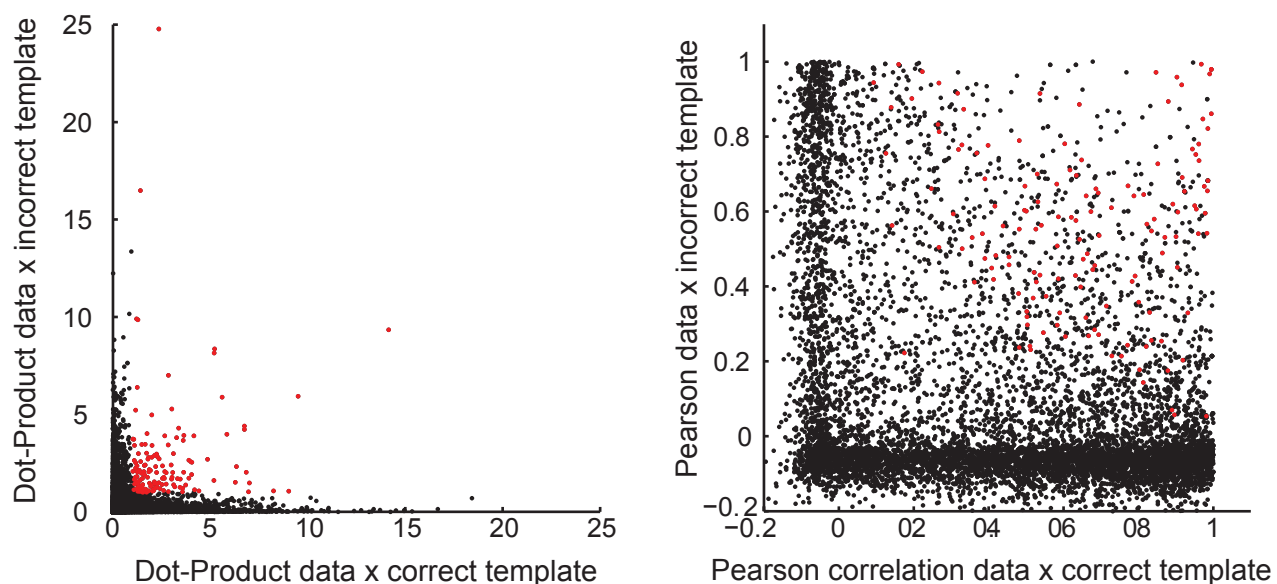


Supplementary Figure 3, Page 1

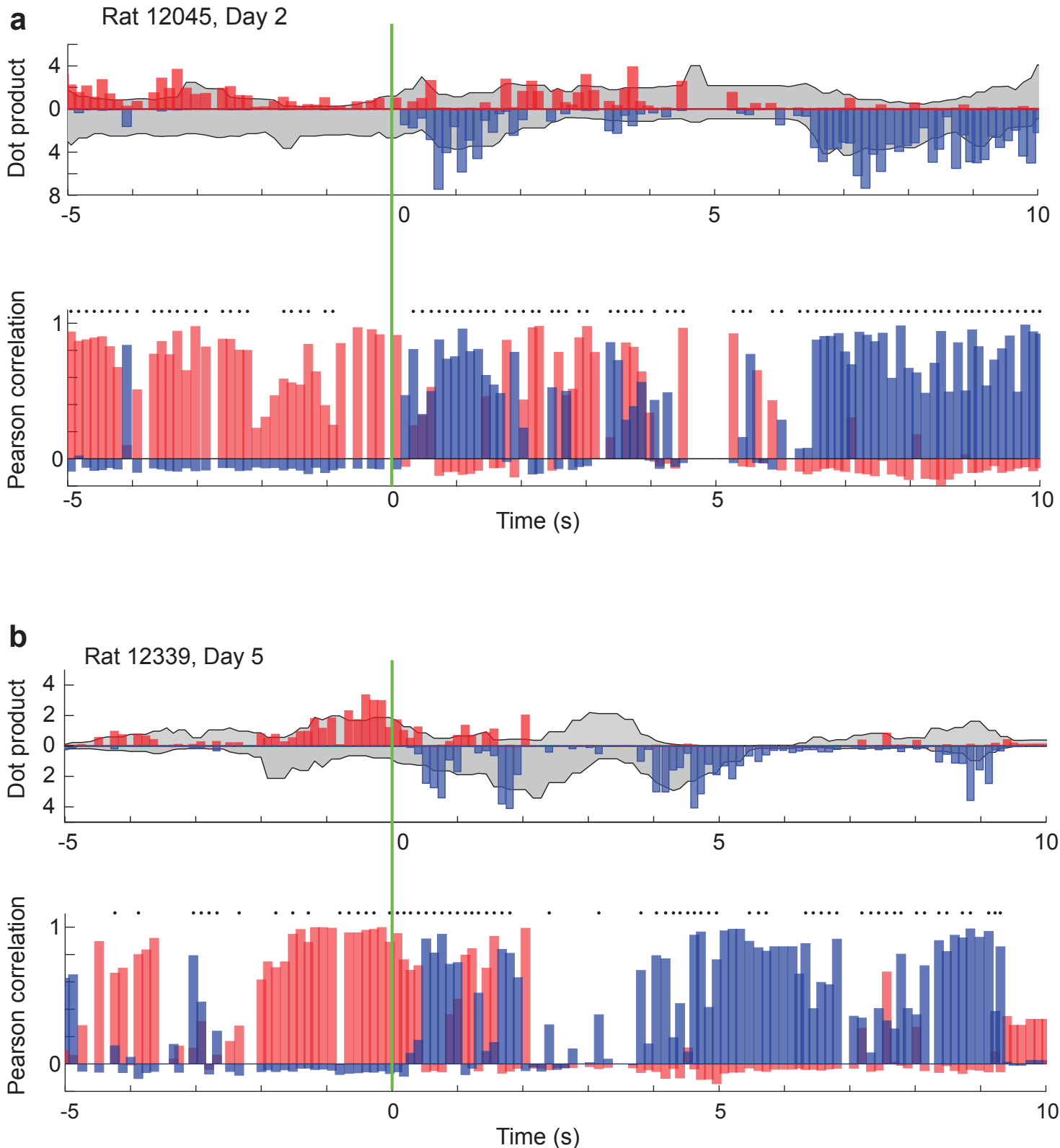


Supplementary Figure 3, Page 2. Transition time-scale. **a.** Example of spiking activity of 43 cells recorded in a 2.5 s post-teleportation period (from rat 12339, Day 5, see Supplementary Fig. 5). **b-d.** To determine if transitions from the current representation (environment II, blue) back to the previous representation (environment I, red) follow the time scale of the theta rhythm, Pearson correlation values were computed between the momentary population activity, shown in **a**, and the corresponding environment I and II representations of that position in the reference environment, generating series of correlations values which differ in the time binning used. Theta periods segmented at the phase of minimal firing were used in **b**, fixed 62.5 ms time bins in **c**, 250 ms ones in **d**. The sequence of environment II correlations (only for bins with at least 2 units active, denoted by black dots) was then cross-correlated with the sequence of environment I correlations (with the same criterion) at a time shift of n time bins, giving $cc(n)$. The single-bin-shifted term $cc(1)$, after subtraction of the cross-correlation at zero time shift $cc(0)$, yielded an estimate of the prevalence of immediate transitions, e.g. transitions from high correlation with environment II and low correlation with environment I in one bin to high correlation with environment I and low correlation with environment II in the next. Temporal bin width affects this difference measure Δcc in several ways, but two main factors, illustrated in the example here, are that for short bin widths, several bins do not qualify for the criterion of having at least 2 units active (**c**); whereas for long bin widths either some transitions are “missed” (such as the one around 106.5 s) or several bins appear to have significant correlation with both representations, thus resulting in apparent mixed states and again lowering the transition count (**d**). Note that also with theta bins (**b**) some mixed cycles are observed, and some transitions are missed due to the 2+ units criterion (the last one in the example shown). **e**, Subtracted cross-correlation values $\Delta cc = cc(1) - cc(0)$ calculated cumulatively over the entire dataset, for fixed bin widths between 44 ms to 500 ms, in the 10 s after each teleportation (filled circles). The figure shows that the largest value for Δcc was obtained at a mean bin width of 125 ms, near the mean length of the theta cycle (120.4 ± 0.9 ms, open diamond). A larger value was obtained for actual theta cycles at the phase of minimum spike activity in the population (0 deg; the point of segmentation between theta cycles used throughout the study), as illustrated in **f**. **f**, Cross-correlation between successive environments I and II representations as a function of theta phase. Correlations with reference environments I and II were determined for successive theta cycles as in Fig. 1b-d and Δcc was calculated as in **e** above. The figure shows the effect of segmentation at different phases of the oscillatory cycle. The phase shift is defined relative to the phase with minimum firing in the cell population (0 deg is the least active phase, as in Fig. 1bc). Note large variability as a function of starting phase. Note also that Δcc is maximal during the first quarter cycle after the phase of minimum firing. Taken together, the analyses suggest that transitions between reference frames are paced by the oscillatory cycle of the theta rhythm.

Note that the modulation in **f** merely reflects the modulation of $cc(0)$ already shown in Fig. 1e. As a function of bin width, however, $cc(0)$, which reflects the prevalence of mixed states, is obviously minimized by using short bins. Therefore, to compare the effects of using actual theta cycles to binning with fixed widths, it makes sense to focus not on mixed states but on how effectively state transitions are revealed, as assessed for example by the subtracted measure $\Delta cc = cc(1) - cc(0)$.

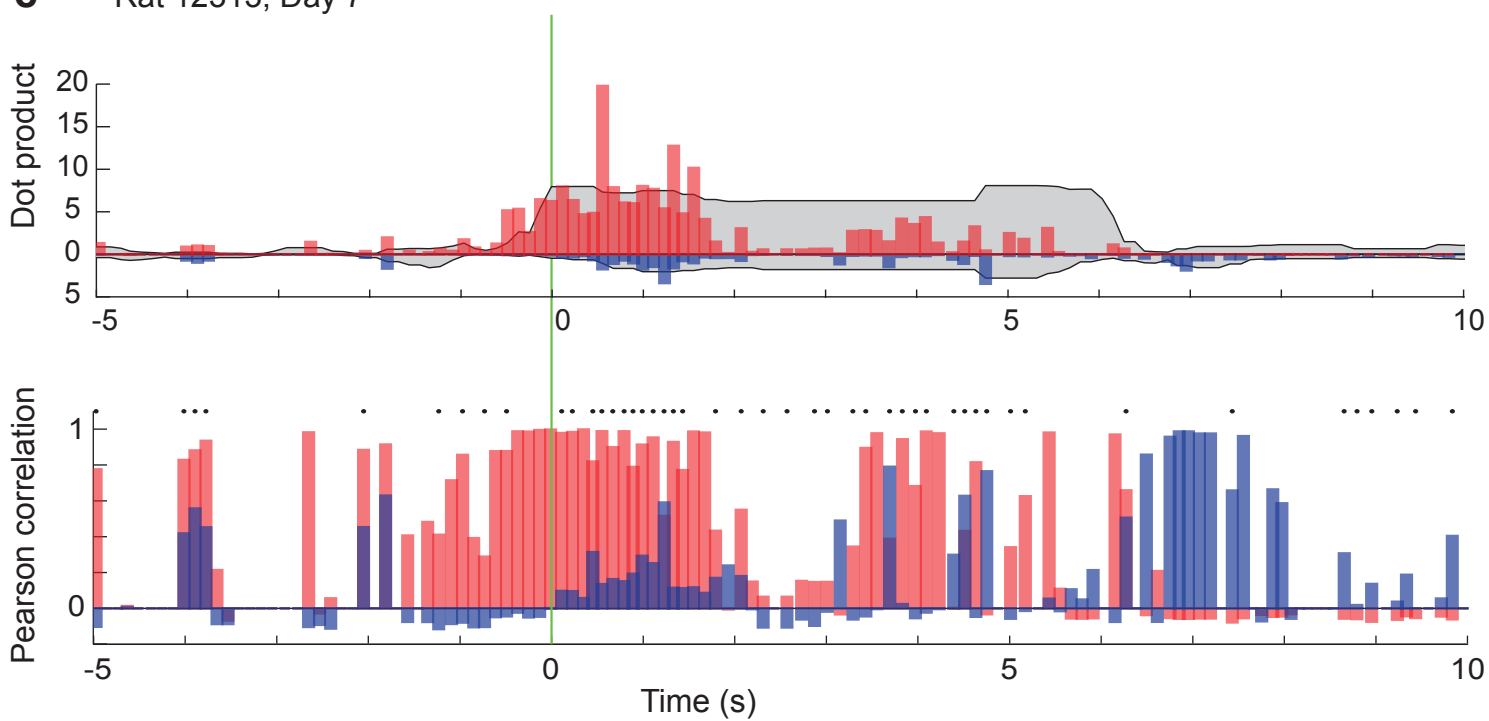


Supplementary Figure 4. Dot-product correlations yield fewer mixed-state theta cycles than Pearson product-moment correlations. The two diagrams compare the number of mixed theta cycles with a dot-product and a Pearson-correlation approach. All theta cycles with 2 or more active cells in all trials of all rats are included. The direction of teleportation is from environment I (original) to environment II (new). Left: Scatterplots comparing the dot product $r \cdot r_{II}/C$ between momentary population vectors during the post-teleportation interval in environment II and reference vectors for the same ‘correct’ environment II (along the x-axis) with the dot product $r \cdot r_I/C$ between momentary post-teleportation population vectors in environment II and reference vectors in the ‘incorrect’ environment I (along the y axis). C is the number of simultaneously recorded units. Reference vectors were taken from the same position in the box as the animal’s current position. Each dot in the scatterplot refers to one theta cycle. Mixed theta cycles, defined as cycles where both $r \cdot r_{II}/C$ and $r \cdot r_I/C$ exceed a value of 1, are indicated in red. Right: The same data analyzed with Pearson product-moment correlations. Correlations between momentary post-teleportation population vectors and reference vectors from the ‘correct’ environment II are shown along the x axis; correlations with the ‘incorrect’ environment I are shown along the y axis. Theta cycles with a ‘mixed’ dot product in the left diagram ($r \cdot r_{II}/C$ and $r \cdot r_I/C$ above 1) are shown in red also in the right diagram. Note that the proportion of theta cycles correlating strongly with both reference environments is substantially larger with Pearson correlations than dot products (i.e., many theta cycles in the upper right quadrant of the scatterplot are not red). The normalization by variance in the Pearson correlation may yield false positives in cases of low variance due to few spikes; thus, we have used the dot product to estimate the frequency of mixed theta cycles in the main text.



Supplementary Figure 5, Page 1

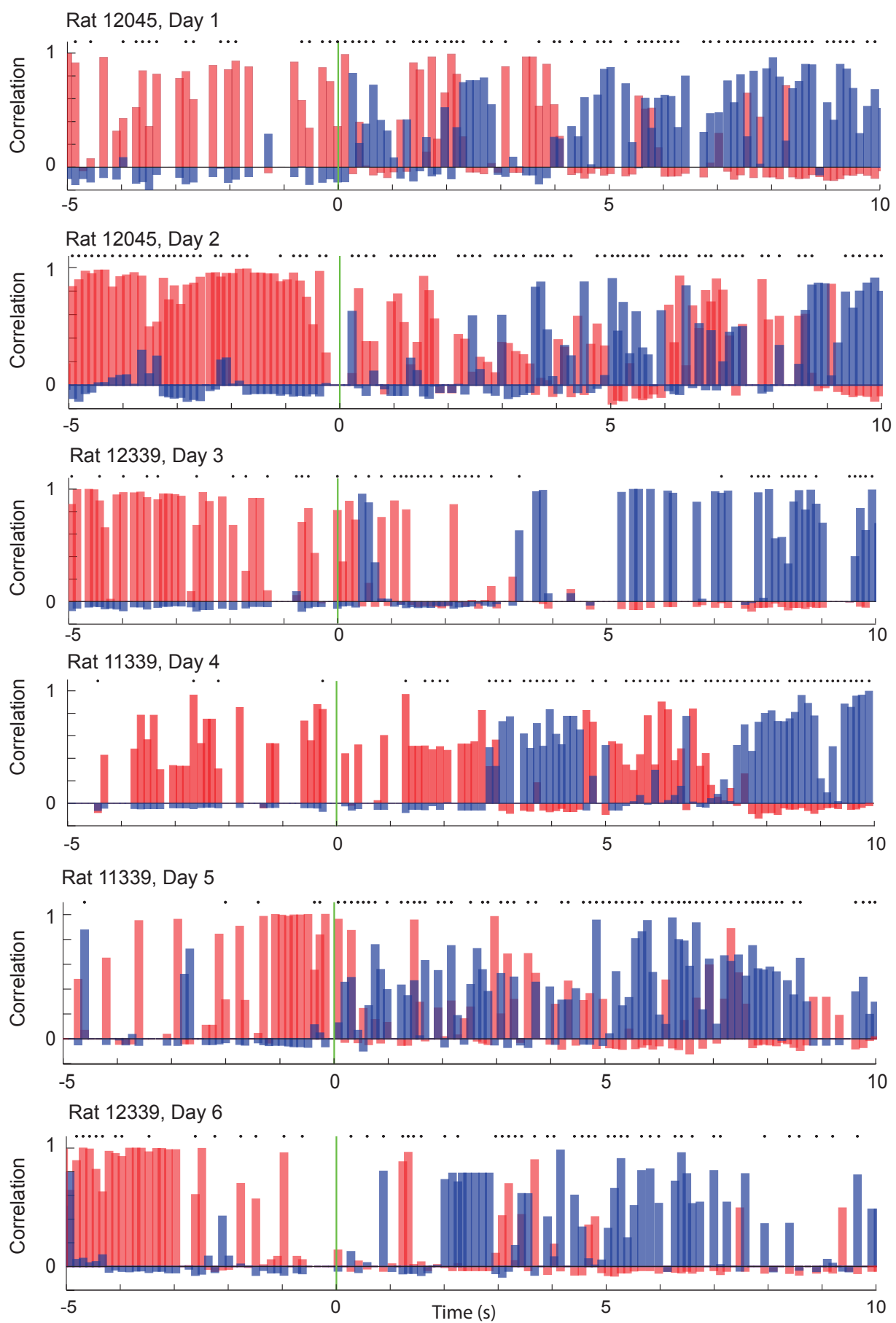
C Rat 12313, Day 7



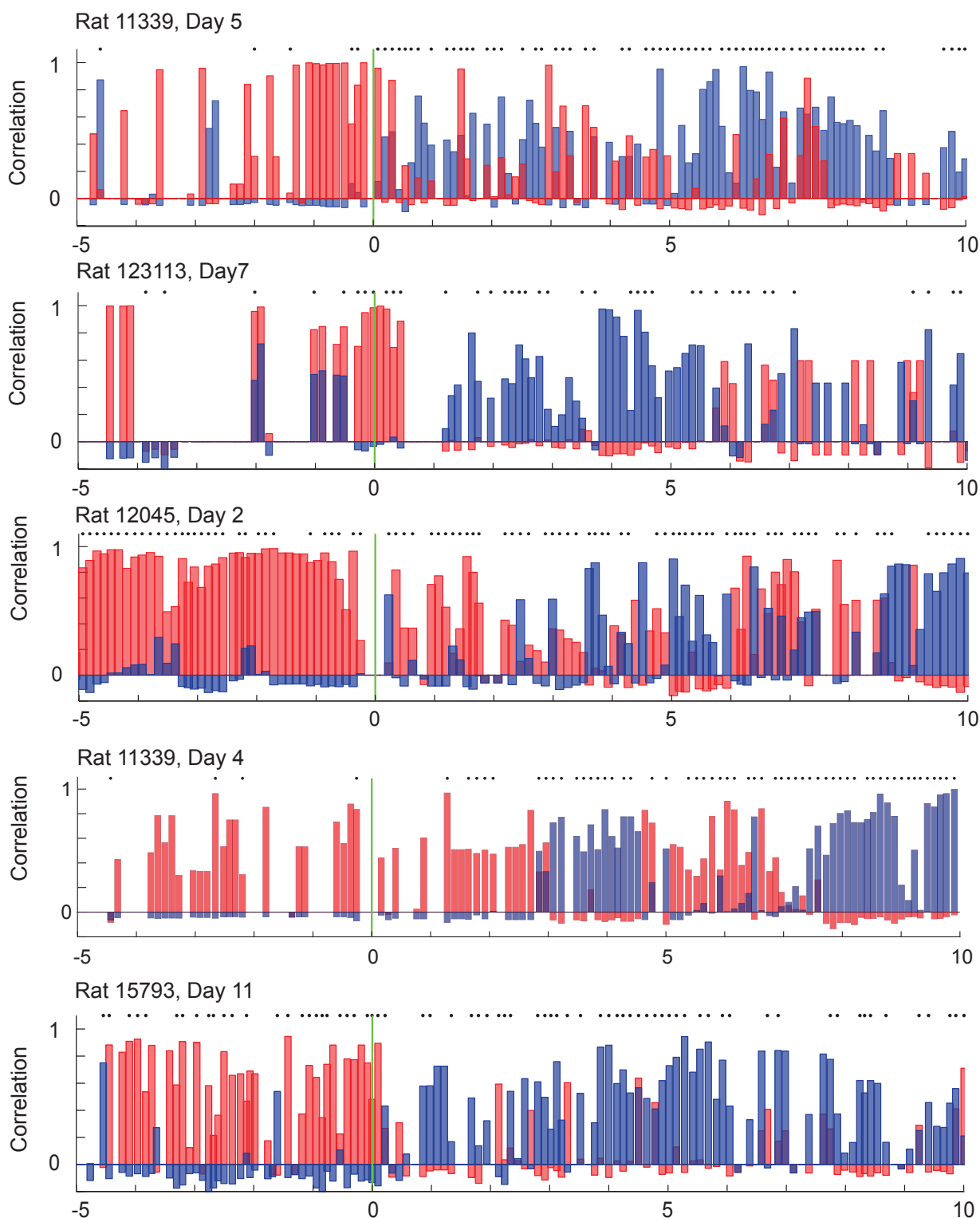
Supplementary Figure 5, Page 2. Comparison of dot-product and Pearson correlation-based estimates of flickering after teleportation (2 pages). Data are shown for 3 teleportation episodes in 3 different animals. Each panel (**a**, **b**, **c**) shows the evolution of population vector correlations after a single teleportation from environment I (before teleportation) to environment II (after teleportation). The top row shows the dot product; the bottom row shows the Pearson product-moment correlation. Vertical bars indicate correlations between momentary population vectors and reference vectors at the current location in I (the original environment; red) and at the same location in II (the new environment; blue). Each bar refers to one theta cycle. The lights were switched at the green vertical line ($t = 0$).

The dot product is divided by the number of recorded cells. All dot products are positive but, for clarity, products with the I and II environments are plotted in opposite directions (up and down, respectively). Dot products are shown against gray shading which indicates the square length of each reference vector, i.e. the dot product with itself. Since the templates are in Hz, and the population vectors for each cycle are spike counts, the reference square is normalized by $1/\text{theta}$ period. The squared dot product of the reference vector provides an indication of the typical dynamic range of the dot products at any given time, though a cycle with strong activity aligned to the reference can yield a dot product well beyond the grey area.

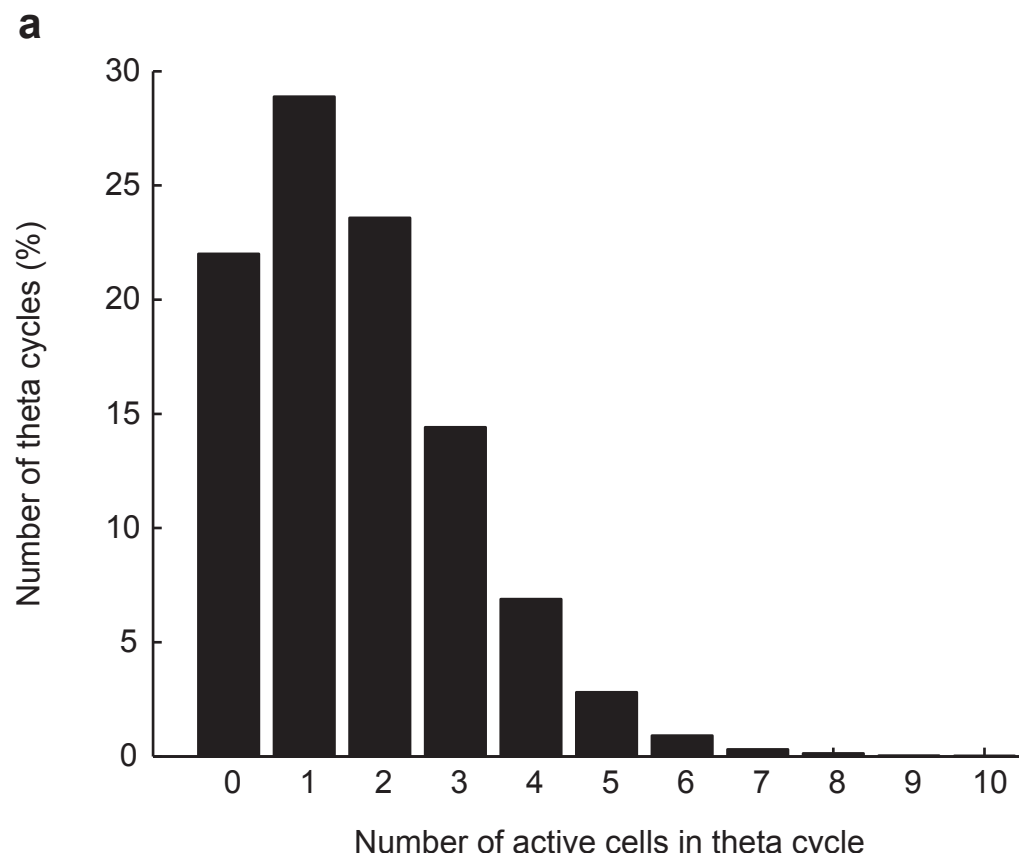
For Pearson correlations, only theta cycles with two or more active cells (marked by black dots above the bars) were included in the analysis. Note that both correlation approaches show frequent flickers after teleportation (short periods of high correlation with the reference vectors for the alternative environment); however the infinite scale of the dot products makes theta cycles harder to compare and flickering difficult to visualize. For this reason we have used Pearson correlations to determine the temporal properties of teleportation-induced flickering. Note also that the momentary population activity is not always orthogonal; panel **c** shows an example where the momentary population vectors correlated with both reference vectors during the initial part of the post-teleportation period (purple bars from 0 to 2 s).



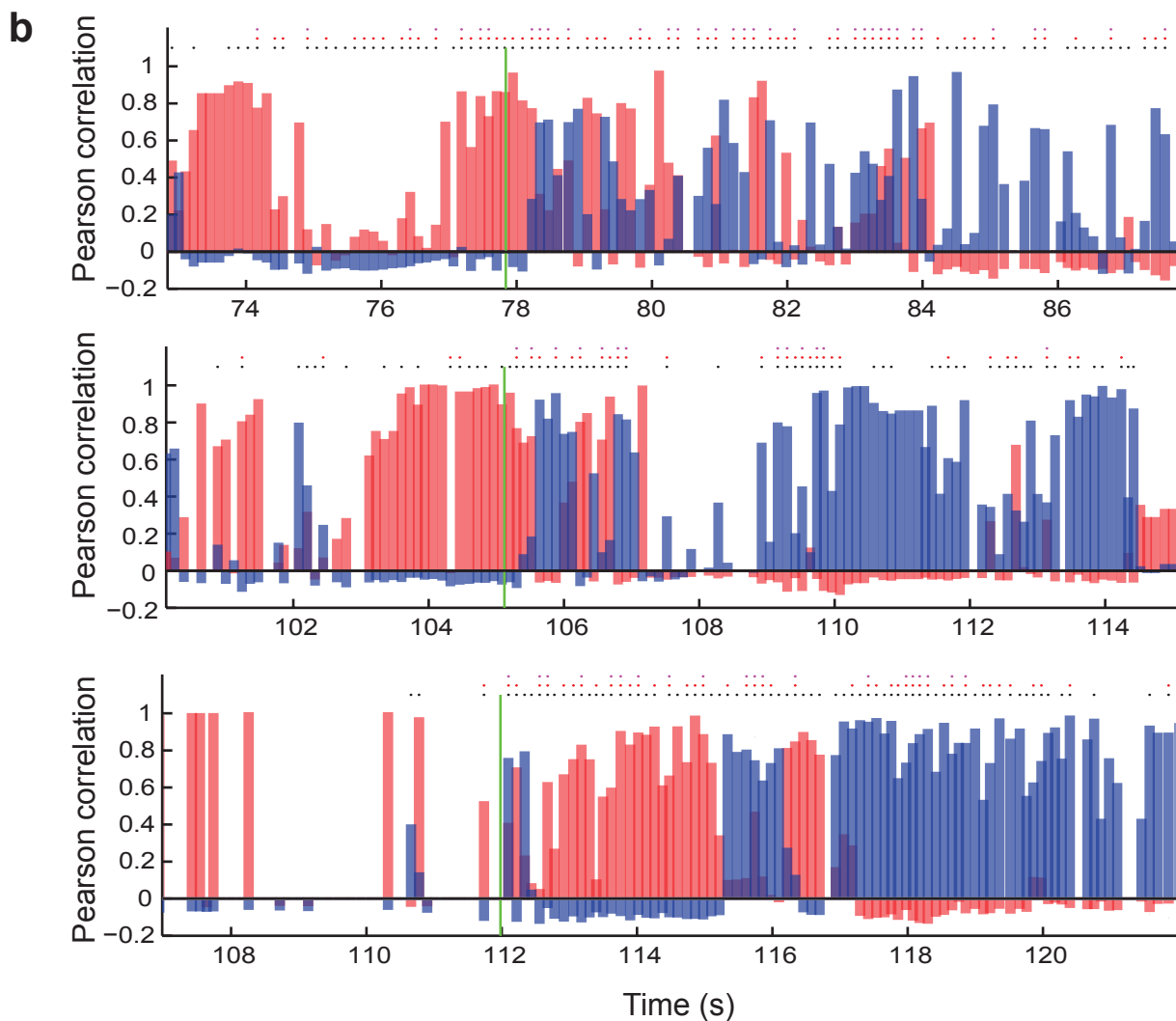
Supplementary Figure 6, Page 1



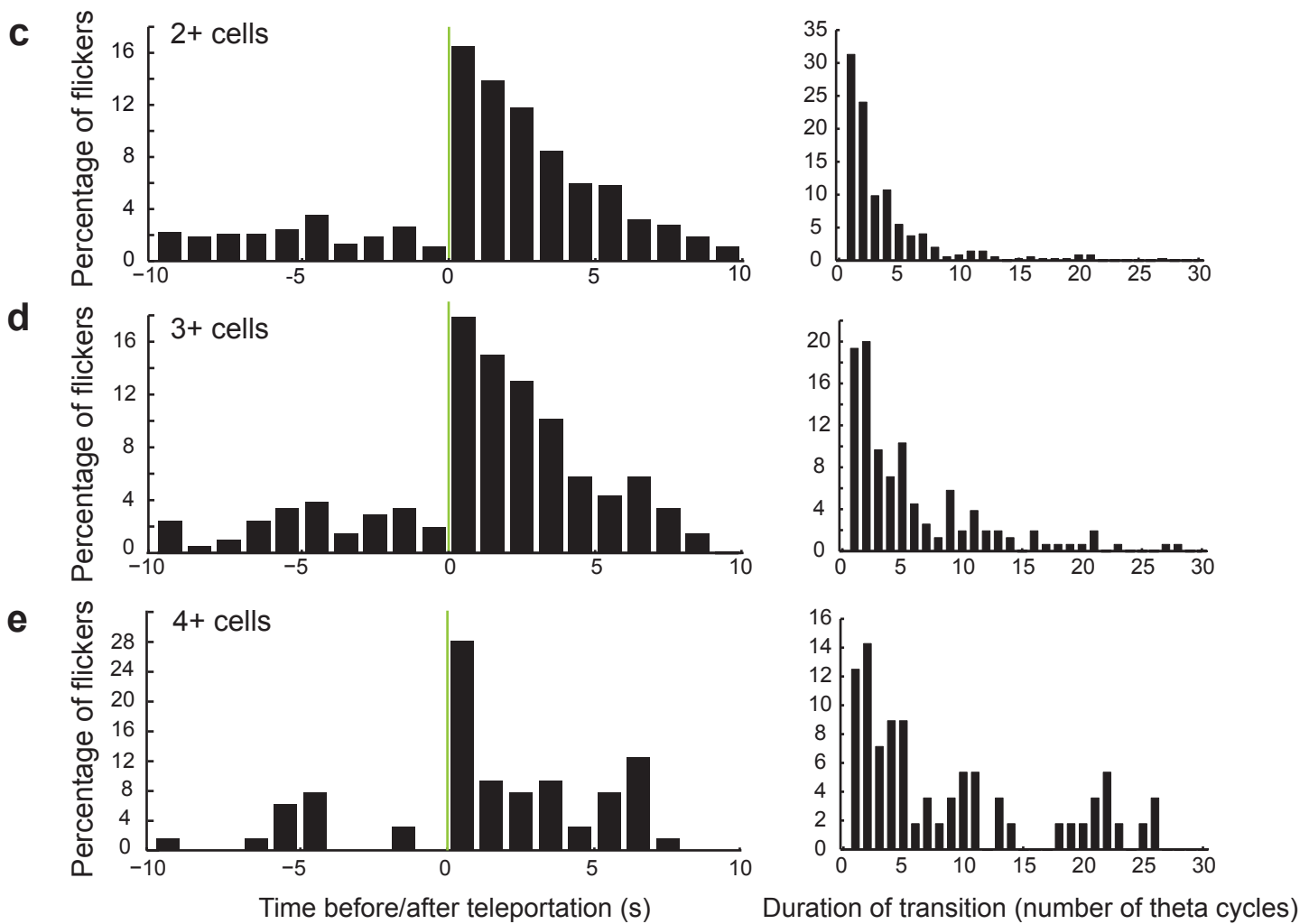
Supplementary Figure 6, Page 2. Additional examples of flickering: one representative episode from each teleportation day in each animal (11 days, 2 pages). Each row shows the evolution of Pearson product-moment correlations between momentary population vectors and reference vectors before and after teleportation from environment I (original) to environment II (new). Reference vectors are taken from the location corresponding to the current position of the animal. Each bar refers to one theta cycle. Red bars indicate correlation with I; blue bars show correlation with II. Only theta cycles with two and more active cells (marked by black dots) were included in the correlation analysis. The lights were switched at the green vertical line.



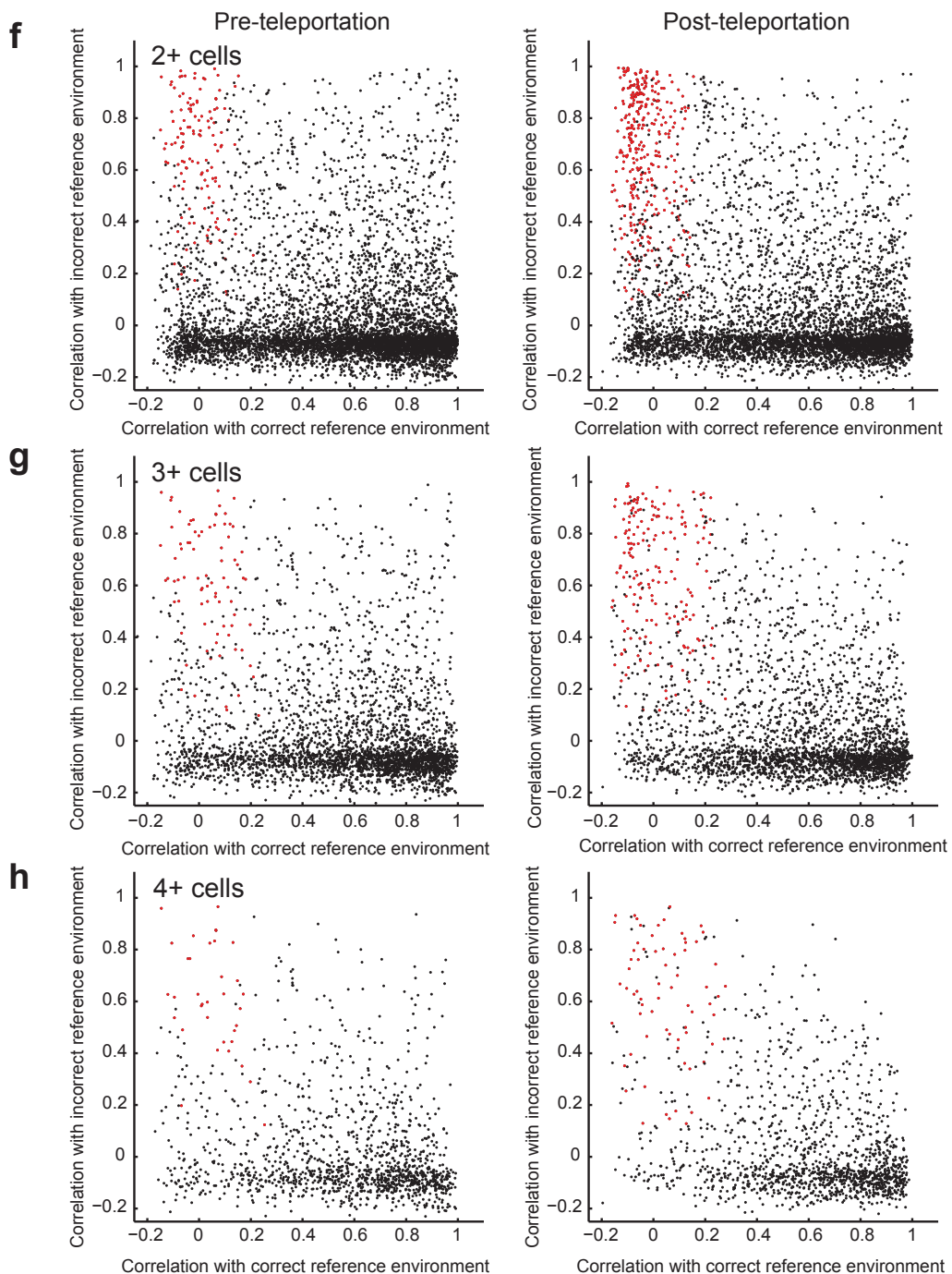
Supplementary Figure 7, Page 1. a, Frequency distribution showing number of active cells per theta cycle during the teleportation period (10 s before and after the switch). Only theta cycles with 2 or more active cells were included in the Pearson product-moment correlation analyses. Analyses with stricter criteria are shown on Page 2 and 3. All active theta cycles were used for the dot product analyses.



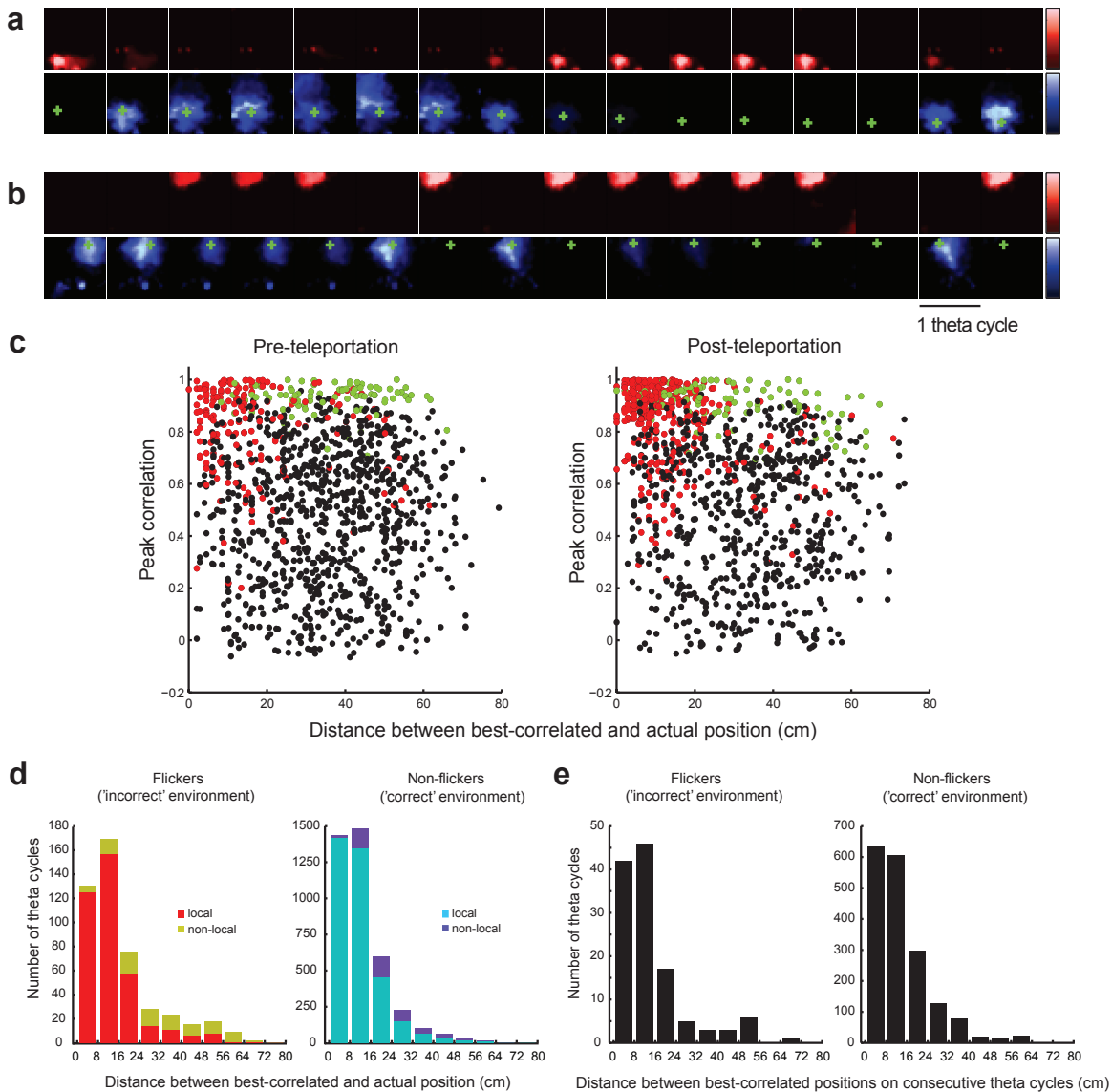
Supplementary Figure 7, Page 2. b, Number of active cells per theta cycle in 3 sequences of flicker events. Each row shows the evolution of Pearson product-moment correlations between momentary population vectors and reference vectors before and after teleportation from environment I (before) to environment II (after), as in Figure 3 and Supplementary Figure 6. Each vertical bar corresponds to one theta cycle. Dots above the bars indicate number of active cells per cycle; black indicates that the 2-cell criterion is satisfied, red that at least 3 cells were active, and purple that at least 4 cells were active. Note that after teleportation (green line), the cell sample tends to alternate between strong correlation with environment I and strong correlation with II even when the criterion is increased to 3 or 4 active cells.



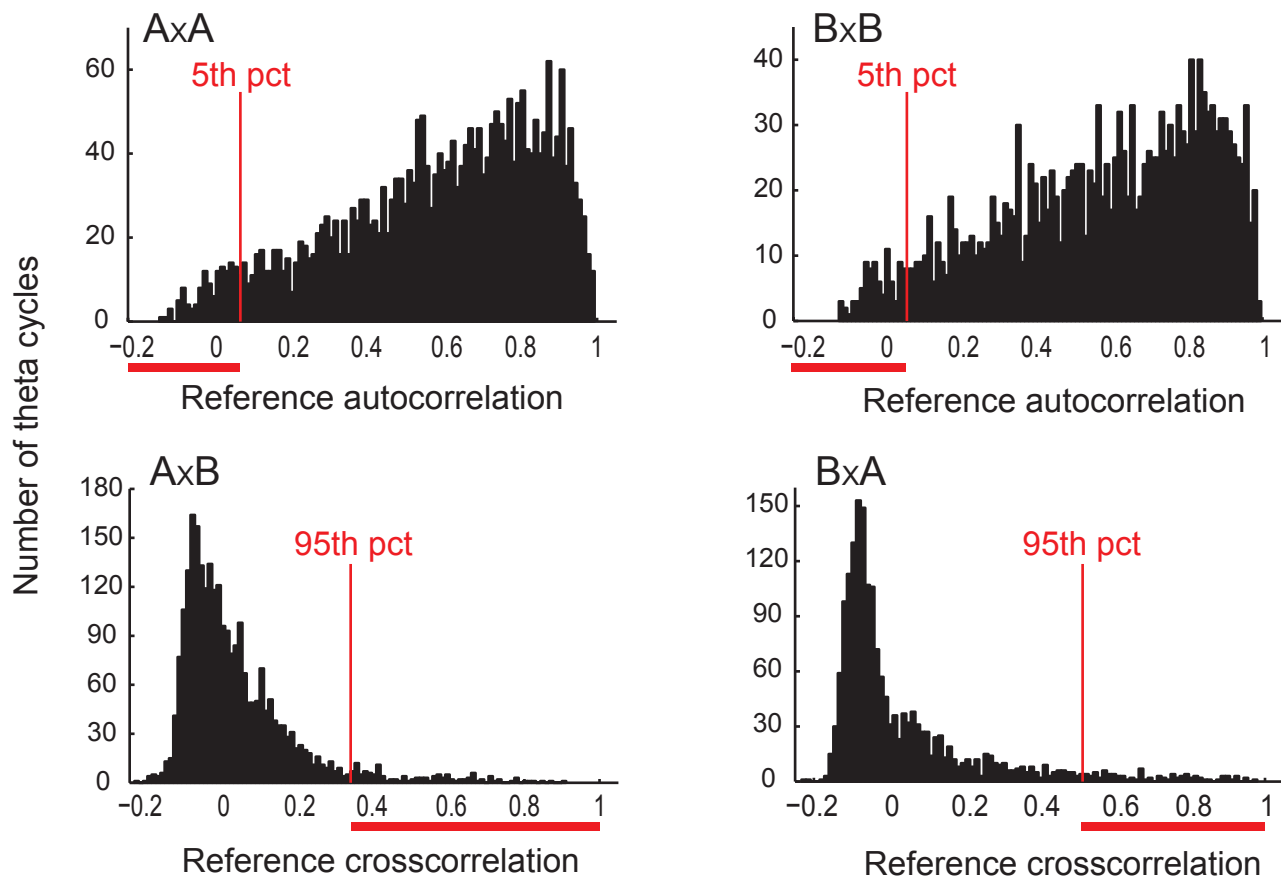
Supplementary Figure 7, Page 3. c-e, Time course of flickering (left) and transition latencies (right) with stricter inclusion criteria (c, all theta cycles with 2 or more active cells; d, cycles with 3 or more active cells; e, cycles with 4 or more active cells). Left column: Frequency distributions showing the percentage of theta cycles flickering to the alternative representation as a function of time before and after teleportation from environment I (before) to environment II (after). Bins are 1 s; green line indicates time of the first switch to the new representation after teleportation. Note increased flickering during the first 5-10 s after teleportation with all three criteria. Right column: Distribution plots showing the time that it takes for the network to switch from an I-correlated to a II-correlated state, or vice versa, measured in number of theta cycles. 1 cycle means that I-correlated and II-correlated cycles were consecutive; longer transition times imply either less direct transitions or that the intervening theta cycles had too few cells to be included. Transitions to the incorrect representation and back to the correct representation were combined. The percentage of flicker events during the 10-s post-teleportation interval did not decrease with the number of simultaneously recorded cells; on the contrary, there was a weak positive correlation ($r=0.171$, d.f. = 147, $P= 0.04$). The persistence of key features of the transition dynamics with stricter criteria (despite the loss of theta cycles) suggests that flickering is not an artifact of small cell samples.



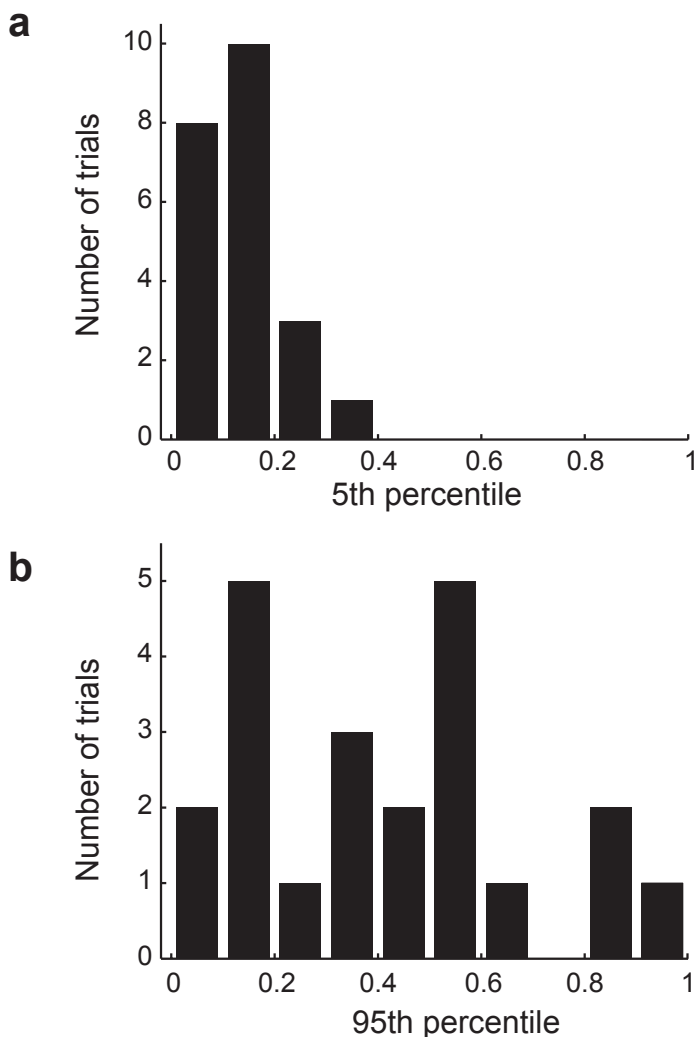
Supplementary Figure 7, Page 4. f-h, Correlation with correct and incorrect environment after stricter inclusion criteria (f, all theta cycles with 2 or more active cells; g, cycles with 3 or more active cells; h, cycles with 4 or more active cells). Each scatterplot compares the Pearson correlation between momentary population vectors and reference vectors for the same ‘correct’ environment (along the x-axis) with the correlation between momentary population vectors and reference vectors in the different ‘incorrect’ environment (along the y axis), as in Supplementary Figure 4 (right panel). Each dot in the scatterplot refers to one theta cycle. Left: Pre-teleportation (10 s). Right: Post-teleportation (10 s from the first switch to the new representation). Red dots indicate theta cycles that pass the criteria for flicker events (defined as in Figure 3d). Note that the number of theta cycles correlated with the incorrect environment increases from pre to post-teleportation with all four selection criteria. The persistence of key features of the transition dynamics with stricter criteria suggests that flickering is not an artifact of small cell samples.



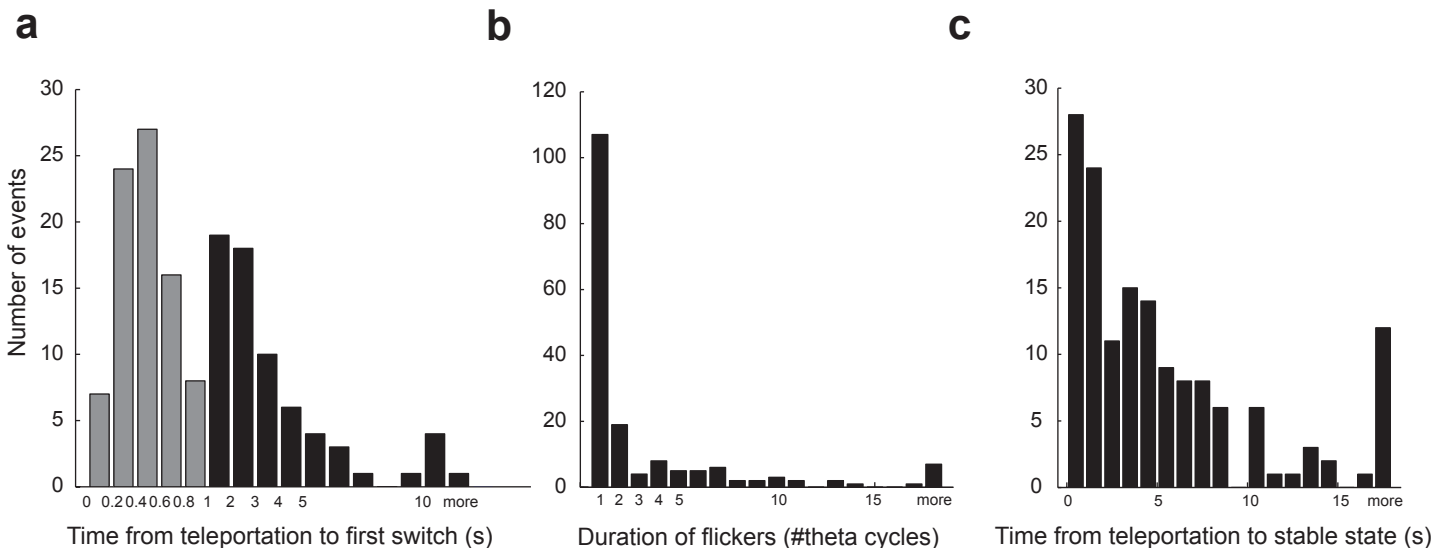
Supplementary Figure 8. Flickers are spatially accurate. **a,b.** Spatial distribution of correlations between momentary population vectors and reference vectors in the two environments after teleportation, as in Fig. 3d. In the example in **b**, theta cycles number 5, 8–10, 13, 15 and 16 did not pass the criterion of two or more active cells per cycle; however, the correlation maps for these cycles are not different from those for the remaining cycles. **c.** Scatterplots comparing momentary population vectors with reference vectors anywhere in the two environments (900 population vectors in each environment). Maximal population vector correlation, obtained anywhere in the reference environment, is shown as a function of distance from the rat's actual location. Each dot refers to one theta cycle. The plot includes all theta cycles from all trials in all animals where the correlation with the current ('correct') environment was below the 5th percentile. Coloured dots refer to flickers to the alternative environment (red: correlation with the non-corresponding reference environment was above the 95th percentile at the rat's location; green: peak correlation was above 95th percentile but correlation at the rat's location was below 95th percentile). Left: 10-s pre-teleportation. Right: 10-s post-teleportation. Note that during flickers the majority of peak correlations remain close to the animal's actual location (distances less than ~20 cm). The percentage of flicker cycles with maximal correlation less than 20 cm from the rat's actual location was 46.5% before teleportation and 73.1% after teleportation. **d.** Distribution of distances between the rat's actual position and the position in the reference environment with the maximal correlation to the momentary population vector. Left: Flickers, i.e. theta cycles with local correlation below the 5-th percentile (5%) with the current environment, and peak correlation above the 95-th percentile (95%) with the alternative environment (all the cycles in colour in panel **c**). The majority of cycles are local flickers where local correlation with the previous environment is above 95%. These are shown in red. Right: Non-flickers, i.e. theta cycles where local correlation with the alternative environment was below 5%, and the peak correlation with the current environment was above 95%. The majority of cycles correlated above 95% with the current environment at the rat's position. These are shown in blue. **e.** Distribution plot showing distance between best-correlated reference vectors on consecutive theta cycles (left, flicker theta cycles, referenced to the incorrect environment; right, theta cycles correlated with the correct environment). Note that also during flicker events, there tends to be consistency from one cycle to the next (distance between best-correlated reference vectors on consecutive cycles: 13.8 ± 1.2 cm for flickers; 13.3 ± 0.3 cm for non-flickers; $Z=0.37$ $P>0.7$, $df=1931$, Wilcoxon rank-sum test). Taken together, the data suggest that activation of representations for remote locations was rare under our test conditions. The fact that the best-correlated population vectors were local also speaks against the possibility that flickers were caused by displacement to another region of a single map (Supplementary Fig. 13).



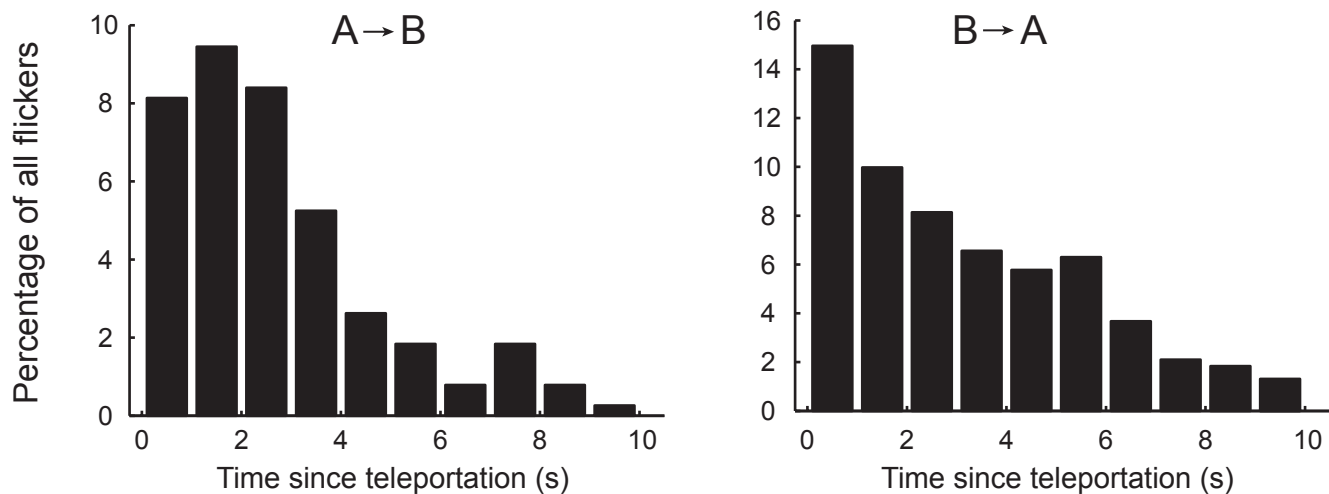
Supplementary Figure 9. Identification of flicker cycles. This figure illustrates the procedure for identifying theta cycles with high similarity to either of the two reference environments (Box A or Box B). Successive theta cycles from reference recordings in A and B were correlated with mean population vectors generated from activity in the same position across the entire reference session in the same environment or in the alternative environment. Distributions show correlations between population vectors referenced to the same environment ($A \times A$ or $B \times B$) or to the alternative environment ($A \times B$ or $B \times A$) in pair of reference trials in one rat. When population vectors are referenced to the same environment ($A \times A$ or $B \times B$), correlations center at high values with a long tail towards the left. When referenced to the alternative environment ($A \times B$ or $B \times A$), the correlations center at slightly negative values with a long tail to the right. Red vertical lines indicate 5th and 95th percentile values. Individual theta cycles were defined as correlated with A if the correlation with Box B was below the 5th percentile threshold of the $B \times B$ reference distribution and the correlation with Box A was above the 95th percentile threshold of the $B \times A$ distribution. Conversely, cycles were defined as correlated with B if the correlation with Box A was below the 5th percentile threshold of the $A \times A$ reference distribution and the correlation with Box B was above the 95th percentile threshold of the $A \times B$ distribution. The red horizontal lines below the panels point to the pairs of correlation values ($A \times A$ and $A \times B$, or $B \times B$ and $B \times A$) that would define a theta cycle as correlated with the alternative environment. Note that the correlation distributions were similar for environments A and B.



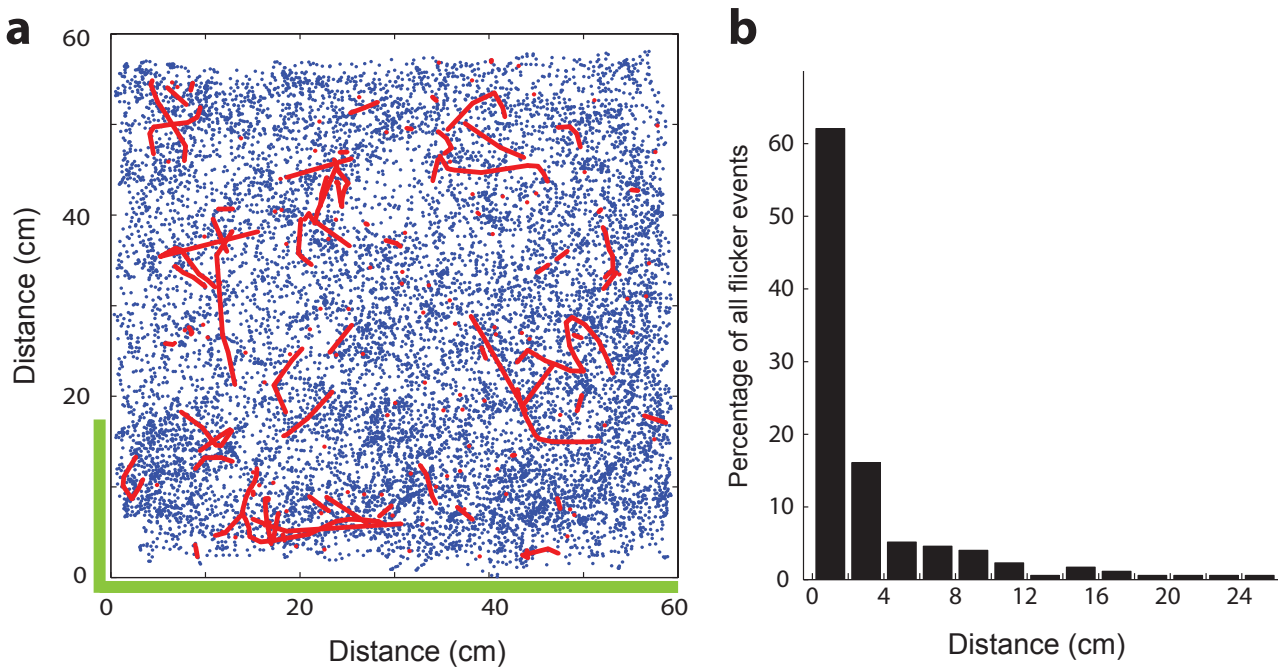
Supplementary Figure 10. *Distribution of the 5th and 95th percentile values used as criteria for identifying flicker cycles.* Theta cycles with high similarity to environments A or B were identified by referencing the population vectors to the same environment as well as the alternative environment. After teleportation from one box to the other, e.g. from A to B, individual theta cycles were defined as A-correlated if the correlation with reference environment A was above the 95th percentile for B×A (i.e. more similar to A than 95% of the theta cycles in B) and if the correlation with reference environment B was below the 5th percentile for B×B (i.e. more different from the reference in B than most theta cycles in B). **a** shows the distribution of 5th percentile values across the entire cell sample (using both teleportation directions); **b** shows the distribution of 95th percentiles (also using both directions). Average 5th percentile values were 0.143 ± 0.015 (mean \pm S.E.M.) whereas average 95th percentile values were 0.411 ± 0.060 (for the two teleportation directions combined). Note very high 95th percentile values (>0.8) in 3 cases, 2 of them originating from the same rat, rat 11892, which had the lowest number of simultaneously active cells ($n=16$). The high threshold in this animal effectively precluded formal detection of flicker cycles, although switches between representations appeared to be present in this animal too (see example in Supplementary Figure 6). The transition latency of this animal was also different (Supplementary Table 1). To be conservative, we included the rat in all analyses reported in the main text. Excluding this animal, in separate analyses, did not significantly affect the pattern of results. Removing all outliers (including the trial from this rat) by restricting the analyses to the two central quartiles of the 95th percentile distribution in **b** did not abolish the increase in flicker frequency (both teleportation directions: $t(97) = 3.81$, $P < 0.001$).



Supplementary Figure 11. Latency and duration of flickers: Group data. **a**, Distribution of latencies from the teleportation event to the first theta cycle correlated with the new reference frame (first II-correlated cycle after teleportation from environment I to II). Note that in the majority of experiments the first transition takes place in less than 1 s. **b**, Distribution of flicker durations. The duration of a flicker was defined as the interval from the first to the last of a series of consecutive theta cycles correlated with the previous environment (using the criterion in Supplementary Fig. 9). **c**, Distribution of latencies from teleportation to reaching a stable state, defined as the first theta cycle at which 10 out of 10 consecutive theta cycles showed higher correlation for the present environment than the previous one. Stable states were generally reached in less than 10 s after the teleportation.

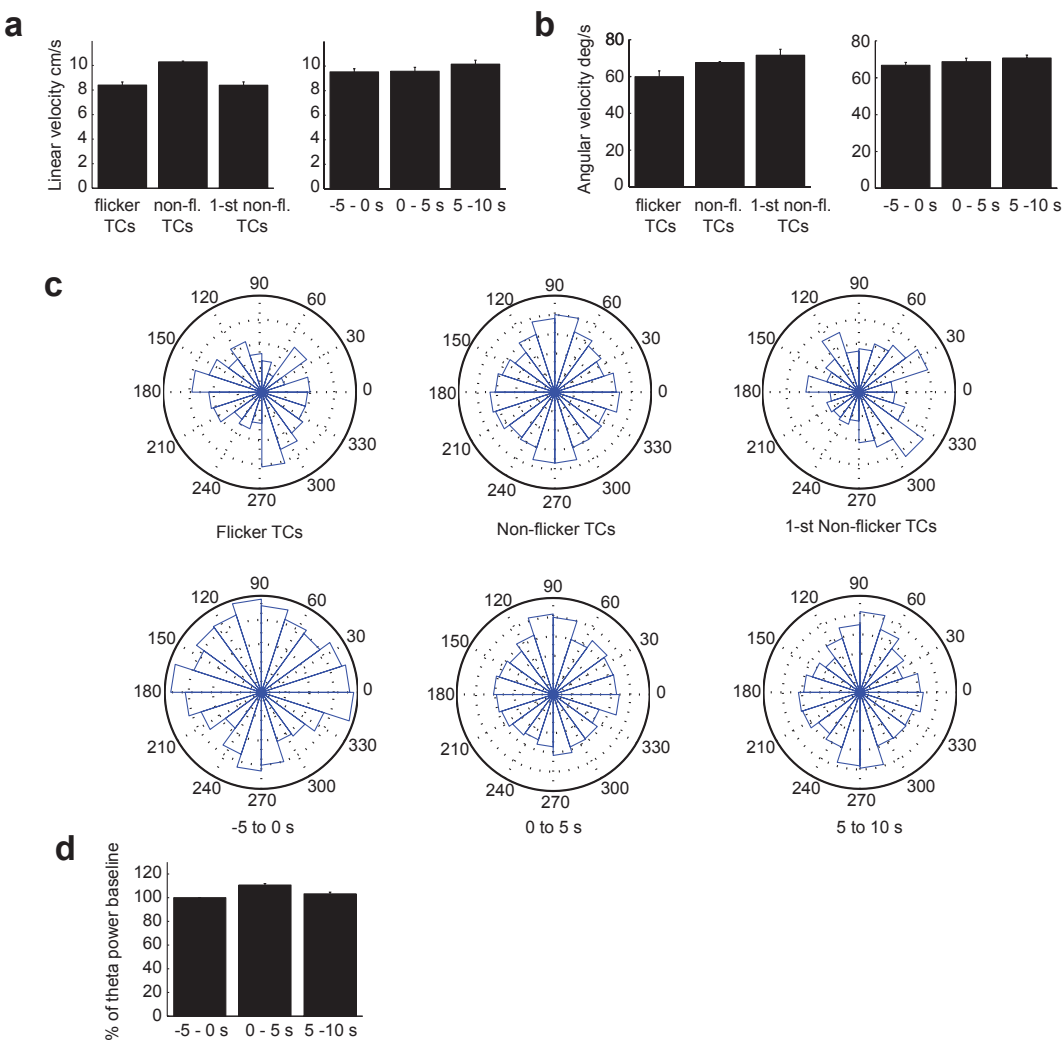


Supplementary Figure 12. Network flickering is independent of teleportation direction. Percentage of flickers as a function of time since teleportation from Box A to Box B (left) and from Box B to Box A (right). Time since teleportation is counted from the first switch to the new representation, usually occurring during the first second after the cue change (Supplementary Fig. 11a). Bin size is 1 s. Flickers were defined as theta cycles for which the correlation between the momentary population vector and the reference vector at the same location in the same environment was lower than the 5th percentile of the distribution of correlations with the corresponding reference environment (red horizontal lines in upper panels), at the same time as the correlation with the reference vector in the alternative environment exceeded the 95th percentile of the distribution of correlations with the noncorresponding reference environment, as illustrated in Supplementary Fig. 9. Flickers are shown as percentages of all flicker events in both directions. The increase in flicker frequency after teleportation was highly significant in both teleportation directions (from Box A to B: $t(72) = 3.32$; from B to A: $t(75) = 3.64$; pooled: $t(148) = 4.92$; all $P \leq 0.001$, paired t-test).

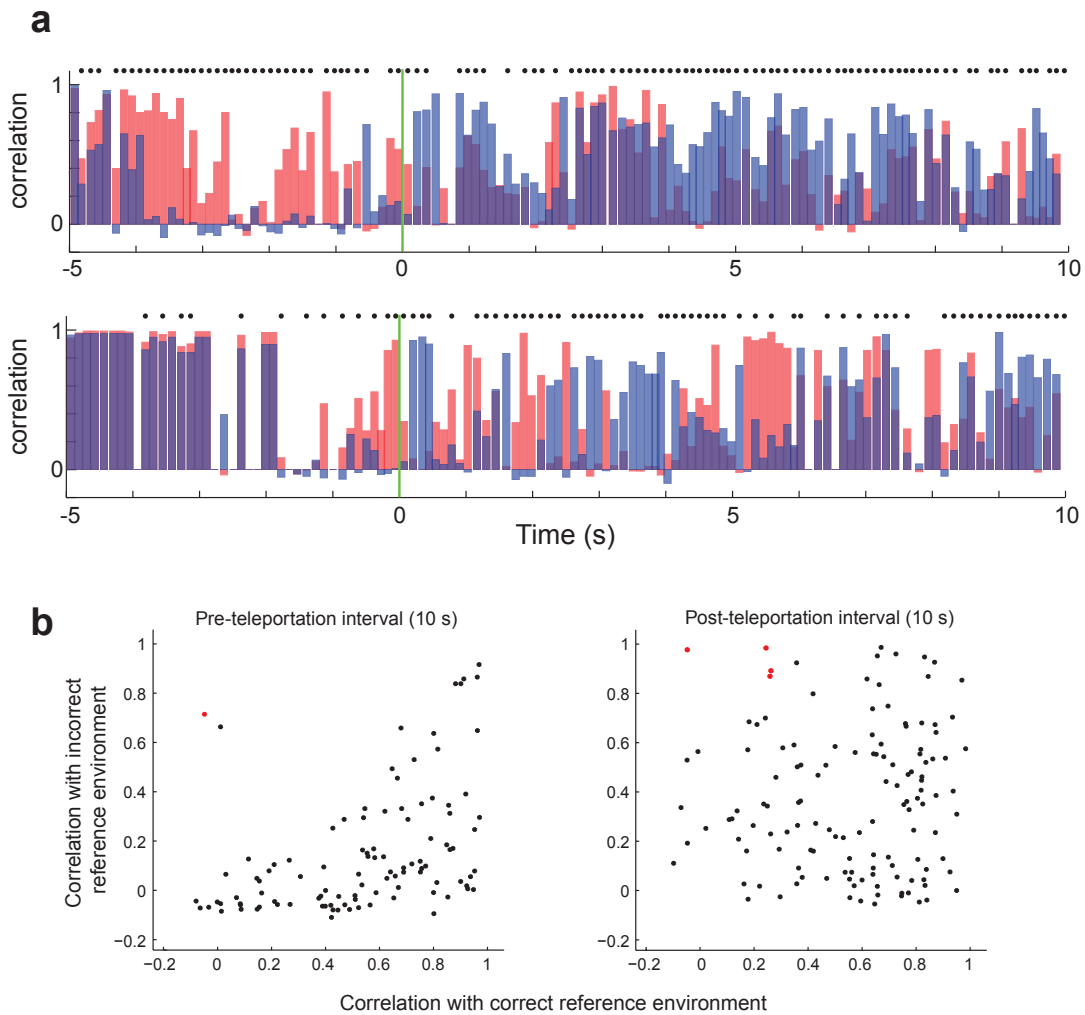


Supplementary Figure 13. *Spatial distribution of flicker events.* **a**, Map of the recording box with the rat's location during all 10-s post-teleportation theta cycles (blue) and during all flicker events, i.e. post-teleportation theta cycles correlated with the pre-teleportation environment (red; Supplementary Fig. 9). Flickers are indicated with dots for single theta cycles and with red lines for non-interrupted sequences of flicker cycles. Note that flickers were distributed across the entire recording box, with no apparent preference for running direction. Green lines indicate positions of light strips in environment B. **b**, Frequency distribution showing the distance that the rats moved during the flicker events. Note that, on approximately 80% of the events, the animals moved less than 4 cm. Orthogonal changes in the population vectors could thus not be caused merely by movement to a region of the box with a different subset of active place cells. Displacement to a different region of the same map is also ruled out by the fact that most ensemble transitions were immediate (Fig. 3f) and the finding that the best-correlated population vector from the incorrect environment generally corresponded to the actual location of the rat (Fig. 3d; Supplementary Fig. 8).

There was no significant correlation between the number of flicker theta cycles and the number of prior teleportations in the present group of animals ($r = -0.036$, $t(147) = 0.44$, $P = 0.66$).



Supplementary Figure 14. Behaviour during flickering. **a**, Left: Linear velocity during all flicker theta cycles (TC), all non-flicker cycles, and the subset of non-flicker cycles immediately succeeding a flicker cycle (means \pm S.E.M.). Running speed was slightly but significantly slower during flicker cycles than non-flicker cycles (8.4 ± 0.3 vs. 10.3 ± 0.1 cm/s, $t(13126)=5.1$, $P<0.001$) but there was no difference between linear velocity during flicker cycles and the first subsequent non-flicker cycle (8.4 ± 0.3 cm/s). Right: Mean linear velocity (\pm S.E.M.) before teleportation and during the first and second block of 5 s after teleportation. There was no significant change in linear velocity between the 5 s before teleportation and the 5 s after teleportation ($t(148)=0.2$, $P>0.8$). **b**, Angular velocity during flicker and non-flicker cycles (as in a). Angular velocity was not significantly different during flicker cycles compared to non-flicker cycles (60.0 ± 3.2 vs. 67.7 ± 0.6 deg/s, $t(13126) = 1.2$, $P>0.2$; first non-flicker theta cycle : 71.7 ± 3.3 deg/s) and there was no significant change in angular velocity from pre-teleportation to post-teleportation ($t(148)=1.3$, $P=0.2$). **c**, Top: Distribution of head direction during all flicker cycles, all non-flicker cycles, and non-flicker cycles immediately succeeding flicker cycles. None of the distributions deviated from uniformity (Rayleigh test: flickers $r=0.07$, $n=381$, $Z=1.87$, $p=0.15$; non-flickers $r=0.003$, $n=12747$, $Z=0.15$, $p=0.86$; first non-flicker theta cycle $r=0.03$, $n=381$, $Z=0.34$, $p=0.71$). Bottom: Distribution of head direction during the 5 s preceding teleportation and the two first blocks of 5 s succeeding teleportation. The mean vector length was small also in these analyses but passed significance because of the very large number of theta cycles (Rayleigh test: 5 s pre-teleportation $r=0.08$, $n=6173$, $Z=40.2$, $P<0.001$; 5 s after teleportation $r=0.07$, $n=6154$, $Z=29.7$, $P<0.001$; 5 to 10 s after teleportation $r=0.02$, $n=6182$, $Z=1.92$, $P=0.15$). The direction of the mean vector during the 5 s after teleportation was towards north, i.e. away from the polarizing green lights (Supplementary Fig. 13a). **d**, Theta power before vs. after teleportation (proportion of pre-teleportation baseline \pm S.E.M.). There was significant increase of theta power between the 5-s block preceding teleportation and the 5-s block succeeding teleportation ($t(148)=5.55$, $P<0.001$).



Supplementary Figure 15. *Flicker events were less distinguishable in CA1.* **a**, Evolution of Pearson population vector correlations after teleportation in simultaneously recorded CA1 cells (last 5 s before teleportation and first 10 s after teleportation; lights were switched at the green vertical line), as in Fig. 3ab. Bars indicate correlations between momentary population vectors and reference vectors at the current location in the original environment (red) and the new environment (blue). Each bar refers to one theta cycle. Black dots mark theta cycles with more than 2 spiking cells. Note high frequency of mixed cycles (purple; cycles that correlate with both reference environments). **b**, Scatterplots comparing correlations between momentary population vectors and reference vectors for the present environment (along the x-axis) with correlations between the momentary population vectors and reference vectors for the previous environment (along the y-axis), as in Supplementary Fig. 4 (right). Reference vectors were taken from the same position in the box that corresponded to the animal's current position. Each dot in the scatterplot refers to one theta cycle. Red dots indicate theta cycles defined as correlated with the alternative environment (flicker cycles; Supplementary Fig. 9). The plot includes all theta cycles with 2 or more active CA1 cells from both teleportation trials recorded in this brain region. Left: 10-s pre-teleportation baseline. Right: 10-s post-teleportation, starting from the first theta cycle correlated with the new environment. The proportion of theta cycles flickering back to the alternative representation was significantly smaller in CA1 than CA3 ($Z=9.37$, $P<0.003$); only 5 theta cycles passed the criterion for flicker events in CA1.

In the CA1 sample, the mean population vector correlation between the reference environments across all position bins was 0.21 ($r=0.013$ in CA3, for comparison). More cells were active in both environments in CA1 than in CA3 ($Z=51.08$, $P<0.01$); the CA1 sample consisted of 37 simultaneously recorded CA1 units recorded over two teleportation trials in the same animal on the same day; 33 of these were active in Box A, 26 in Box B, and 22 in both environments (spatial correlation $r=0.19 \pm 0.04$, mean \pm S.E.M.).

Rat	Time to first state change (s)		Time to stable state (s)		Flicker duration (TC)	
	25 th pct	75 th pct	25 th pct	75 th pct	25 th pct	75 th pct
11892	3.87	5.55	4.26	9.35	NaN	NaN
12045	0.41	2.50	3.25	7.50	1	5
12313	0.49	1.06	2.78	20.00	1	1
12339	0.44	2.56	1.19	6.33	1	3
15792	0.40	1.58	1.27	6.22	1	1
15793	0.42	1.74	0.79	3.13	1	1

Supplementary Table 1. Latency and duration of flicker events in individual animals